Computer Methods in Applied Mechanics and Engineering 453 (2026) 118823

Contents lists available at ScienceDirect

Comput. Methods Appl. Mech. Engrg.

journal homepage: www.elsevier.com/locate/cma

The virtual element method for arbitrarily distorted 8-node bricks

M. Cremonesi [a], F. Dassi [b], C. Lovadina [c,d], U. Perego [a], A. Russo [b,d,*]

[a] Department of Civil and Environmental Engineering, Politecnico di Milano, Milan, 20133, Italy
[b] Department of Mathematics and Applications, University of Milano-Bicocca, Milan, 20133, Italy
[c] Department of Mathematics, University of Milano, Milan, 20133, Italy
[d] IMATI-CNR, Pavia, 27100, Italy

ARTICLE INFO

Keywords:
Finite element method
Virtual element method
8-Node isoparametric brick elements
Hexahedral virtual elements with curved faces

ABSTRACT

Standard isoparametric 8-node hexahedral Finite Elements (FEs) are among the most widely used elements for the simulation of 3D problems. While these elements provide excellent results in the case of regular meshes, their accuracy may deteriorate with increasing distortion, finally failing in the case of degenerate elements, where the Jacobian determinant of the geometry mapping vanishes inside the element. In the case of simulation domains of complex geometries, the generation of a mesh of regular or only mildly distorted brick elements can be extremely difficult and time consuming, and in some cases it is even impossible to obtain a mesh free of degenerate elements. Three-dimensional Virtual Elements (VEs) are well known to be highly robust with respect to extreme element distortion; however, at least in the conforming setting, they are restricted to polyhedral elements with planar faces. To enhance the usability of VEs and to make possible their integration in meshes of FE isoparametric bricks, thus significantly reducing the meshing time, in this work we formulate a new 8-node, order 1, hexahedral VE with curved faces, that we name *virtual brick*. With reference to a simple reaction-diffusion problem, it is shown that the proposed element is convergent and fully compatible with regular 8-node isoparametric FEs. Furthermore, the integrals on the element faces and volume can be computed using the standard Gauss quadrature rules of the isoparametric FE, a property of great importance in the case of nonlinear problems. All these properties hold also in the degenerate case, as long as the virtual brick faces do not intersect with each other.

1. Introduction

In engineering applications, the standard isoparametric Finite Element Method (i.e. based only on primal variational formulations) is one of the most widely used and effective approaches for solving partial differential equations. Its popularity stems from its flexibility in handling complex geometries and its direct implementation within the Galerkin framework. However, the performance of the isoparametric FEM depends on the mesh quality, and it faces significant challenges when the elements deviate from an ideal configuration.

The most common types of elements used for practical engineering continuum-based problems are isoparametric triangles or quadrilaterals in 2D and tetrahedral or hexahedral elements in 3D. Despite the fact that hexahedral mesh generation algorithms are less general and effective (for a complex model, creating a hexahedral mesh can take much longer than a corresponding tetrahedral mesh

* Corresponding author.
E-mail addresses: massimiliano.cremonesi@polimi.it (M. Cremonesi), franco.dassi@unimib.it (F. Dassi), carlo.lovadina@unimi.it (C. Lovadina), umberto.perego@polimi.it (U. Perego), alessandro.russo@unimib.it (A. Russo).

https://doi.org/10.1016/j.cma.2026.118823
Received 19 December 2025; Received in revised form 6 February 2026; Accepted 8 February 2026
Available online 14 February 2026

[1,2]), hexahedral meshes are often preferred because they typically require from 4 to 10 times less elements than a tetrahedral mesh to obtain the same level of accuracy [1,3]. When these isoparametric elements are distorted, e.g. skewed, stretched or collapsed, the mapping from the reference element to the current element deteriorates, possibly affecting the approximation of the solution fields [4,5] and of their gradients [6], especially in the case of coarse meshes. A key requirement of the method is that the Jacobian determinant of the mapping remains above zero throughout the element, so that the mapping is invertible. Elements with a Jacobian determinant changing sign inside the element, such as concave elements in 2D and folded elements in 3D, are said to be degenerate. Poor-quality meshes can produce small Jacobian determinant values, leading to numerical instabilities and, when they contain degenerate elements, to complete failure of the simulation.

A common strategy to mitigate these issues is to use mesh improvement algorithms to eliminate distorted elements, based on suitable distortion metrics [3,7]. However, these techniques may be computationally demanding, requiring significant user interaction, and possibly not capable of producing meshes free from degenerate elements in the case of extremely complex domains [8]. An alternative approach is to retain the distorted mesh and adapt the solution method. Examples in this line are the different variants of hybrid or mixed finite element methods, or methods based on reduced integration with stabilization. See [9], and references therein, for a review on mixed and enhanced strain methods (see also e.g. [10,11] for other approaches). In this respect, the Virtual Element Method (VEM) [12] is of particular interest, since it operates directly on the physical element, without resorting to a geometry mapping from a parent element and, therefore, it is free from the problems connected with the mapping inversion, such as those related to the vanishing of the Jacobian determinant. For a recent review of the VEM, see [13]. Despite its high tolerance to distortion, even for elements of arbitrary and nonconvex shape, the Virtual Element Method (VEM) in three dimensions in the conforming setting is limited to polyhedral elements, i.e. elements with an arbitrary number of planar polygonal faces (see [14]). An attempt to overcome this difficulty is described in [15], where, however, only one curved face per polyhedron is allowed. For the nonconforming setting some preliminary results can be found in [16].

Given the previous limitations, while there have been proposals of 2D Virtual Elements (VEs) with curved edges [17–19], all the 3D VEM applications proposed so far in the literature make use of polyhedral elements. An attempt to overcome the limitation of flat faces in the case of hexahedral elements has been presented in [20], where 12-faces "Deltahedral" brick VEs have been formulated, with each quadrilateral face subdivided into two triangles. Other examples of 3D applications of the VEM with polyhedral elements to solid mechanics are, e.g., [21] for linear elasticity, [22] for linear elastic elastodynamics, [23–25] for large strains hyperelasticity, [26–28] for large strain plasticity.

Another difficulty with the implementation of the VEM is the need to stabilize the stiffness matrix. The standard VEM stabilization is known to potentially produce a loss of accuracy in the presence of highly distorted VEs [29]. For this reason, the formulation of self-stabilized (or stabilization-free) VEs is gaining increasing popularity (see, e.g., [30–32] for self-stabilized VEM in 2D and [20,33,34] in 3D) and is pursued also in the present work.

To tackle the problem of element distortion, to overcome the 3D VEM limitation to elements with flat faces and to allow for a seamless integration of VEs in a finite element mesh of hexahedral elements, in this work we introduce a new hexahedral self-stabilized VE, possibly degenerate, with curved quadrilateral faces, which we call the *virtual brick*. A virtual brick is defined as a solid with six quadrilateral faces that are bilinear transformations of the reference square, without relying on the trilinear mapping used for the interior of the element. The face functional space coincides with that of the standard 8-node isoparametric brick. Our approach has the following features.

- The virtual brick is extremely robust with respect to mesh distortion, a property already observed for the VEs in many other situations.
- Full compatibility between virtual bricks and classical Finite Element (FE) bricks is ensured, which means that virtual bricks can be easily integrated into standard meshes of FE bricks.
- Since the virtual brick is based on the same degrees of freedom of the FE isoparametric brick element, the virtual brick seamlessly supports adaptive strategies that selectively employ VEM only in regions with highly distorted or degenerate elements, while maintaining conventional FEs elsewhere.
- The standard quadrature rules based on Gauss points, commonly used in the FEM, can be used also for our virtual bricks, both for the volume and surface integrals, a feature which is particularly important in view of a possible extension to nonlinear applications.

As a proof of concept, in this work, the proposed method is applied to a simple thermal problem with a reaction term and, with the aid of numerical tests, we will show how these capabilities provide a robust and versatile framework for complex three-dimensional simulations. The paper is organized as follows.

In Section 2 we recall the definition of the standard isoparametric brick FE, while in Section 3 we introduce a suitable definition of the virtual brick. For such a virtual brick, in Section 4 we construct a virtual space, by considering a suitable extension of the isoparametric bilinear functions defined on the brick faces. To this aim, we introduce the typical VEM polynomial projector Π_1^∇ and discuss its computability. Section 5 is devoted to the integration of functions defined on a virtual brick. In Section 6 we present the discretization of the thermal problem in this framework, also considering a self-stabilized formulation. Section 7 deals with the method convergence: under suitable hypotheses (quite classical in the framework of the VEM theoretical analysis), we state the theorems which show the optimal convergence rate of the scheme. Finally, the numerical results are presented in Section 8.

Throughout the paper, we employ rather standard notation. In particular, in Sections 5 and 7 we use classical notation for the functional spaces, see e.g. [35]. However, we remark that vectors in $\mathbb{R}^3$ are denoted by bold symbols, while vectors in $\mathbb{R}^2$ are always indicated in components. Furthermore, Latin indices $i, j, k, \dots$ will range from 1 to 8 while Greek indices $\alpha, \beta, \dots$ will range from 1 to 4.

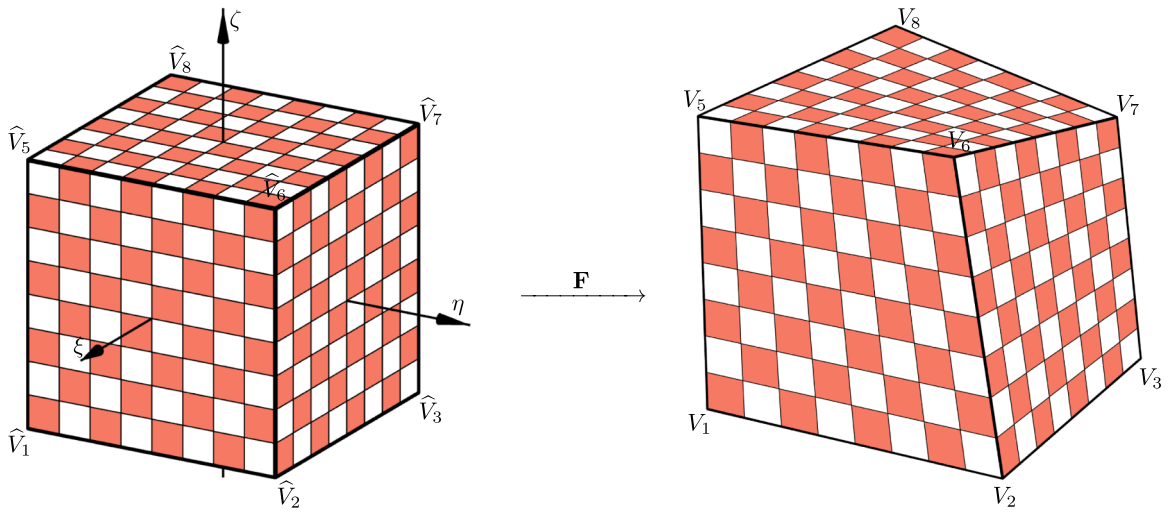

(a) Reference cube $\widehat{\mathcal{B}}$ (b) 8-node brick $\mathcal{B}$

Fig. 1. The trilinear map **F**.

2. The isoparametric 8-node brick

In this Section, we briefly recall the standard isoparametric 8-node brick. All quantities referring to the reference biunit cube or square will be denoted by a superposed hat.

We start by defining the reference biunit cube $\widehat{\mathcal{B}} := [-1,+1]^3 \subset \mathbb{R}^3$, with vertices $\widehat{V}_i = (\xi_i, \eta_i, \zeta_i)$, $i = 1, \dots, 8$, given by

$$\begin{aligned} \widehat{V}_1 &= \begin{bmatrix} -1 \\ -1 \\ -1 \end{bmatrix}, \ \widehat{V}_2 = \begin{bmatrix} +1 \\ -1 \\ -1 \end{bmatrix}, \ \widehat{V}_3 = \begin{bmatrix} +1 \\ +1 \\ -1 \end{bmatrix}, \ \widehat{V}_4 = \begin{bmatrix} -1 \\ +1 \\ -1 \end{bmatrix} \\ \widehat{V}_5 &= \begin{bmatrix} -1 \\ -1 \\ +1 \end{bmatrix}, \ \widehat{V}_6 = \begin{bmatrix} +1 \\ -1 \\ +1 \end{bmatrix}, \ \widehat{V}_7 = \begin{bmatrix} +1 \\ +1 \\ +1 \end{bmatrix}, \ \widehat{V}_8 = \begin{bmatrix} -1 \\ +1 \\ +1 \end{bmatrix}. \end{aligned} \tag{1}$$

The corresponding reference trilinear shape functions $\widehat{N}_i(\xi, \eta, \zeta)$ are defined on $\widehat{\mathcal{B}}$ by

$$\widehat{N}_i(\xi, \eta, \zeta) := \frac{1}{8}(1 + \xi_i\xi)(1 + \eta_i\eta)(1 + \zeta_i\zeta) \tag{2}$$

and have the property $\widehat{N}_i(\widehat{V}_j) = \delta_{ij}$. Given 8 ordered points V_i, $i = 1, \dots, 8$ in $\mathbb{R}^3$, we define the trilinear map $\mathbf{F} : \widehat{\mathcal{B}} \to \mathbb{R}^3$ as

$$\mathbf{F}(\xi, \eta, \zeta) := \sum_{i=1}^{8} \widehat{N}_i(\xi, \eta, \zeta) V_i. \tag{3}$$

It is clear that by construction $\mathbf{F}(\widehat{V}_i) = V_i$. If $\det J_{\mathbf{F}}(\xi, \eta, \zeta) > 0$ for $(\xi, \eta, \zeta) \in \widehat{\mathcal{B}}$, the map $\mathbf{F} : \widehat{\mathcal{B}} \to \mathbf{F}(\widehat{\mathcal{B}})$ is an invertible transformation and we define the 8-node isoparametric brick element $\mathcal{B}$ as the image of $\widehat{\mathcal{B}}$ through **F**, i.e. $\mathcal{B} := \mathbf{F}(\widehat{\mathcal{B}})$. In this case, $\mathcal{B}$ is a standard 8-node brick element in space; its skeleton is made of straight edges while faces in general are curved, see Fig. 1.

Definition 1. A *regular brick* $\mathcal{B}$ is the image of $\widehat{\mathcal{B}}$ through **F** when $\det J_{\mathbf{F}}(\xi, \eta, \zeta) > 0$ for all $(\xi, \eta, \zeta) \in \widehat{\mathcal{B}}$.

Note that in this work, a brick element is considered *degenerate* (in opposition to *regular*) when the Jacobian determinant of the geometry mapping is negative in some parts of the element volume. However, the accuracy is known to degrade as this limit distortion is approached and therefore different definitions of degeneration can be found in the literature.

By direct computation, it can be seen that the determinant of the Jacobian of **F** is a polynomial in (ξ, η, ζ) of at most second degree in each variable, yet in every monomial only one variable can appear with exponent 2: for instance, $\xi\eta^2\zeta$ and $\xi^2\zeta$ can be present, but $\xi^2\eta^2\zeta$ cannot.

It is not straightforward to give sufficient conditions on the location of the vertices V_i ensuring that the corresponding brick is regular; an efficient algorithm can be found in [36]. It has been shown in [37] that it is not even enough to check that $\det J_{\mathbf{F}}$ is positive on all edges to ensure that it is positive everywhere.

The situation is much easier in two dimensions: the determinant of the Jacobian of the transformation is a first-order polynomial and a quadrilateral is regular in the sense of Definition 1 if and only if it is convex; furthermore, it is enough to check that the

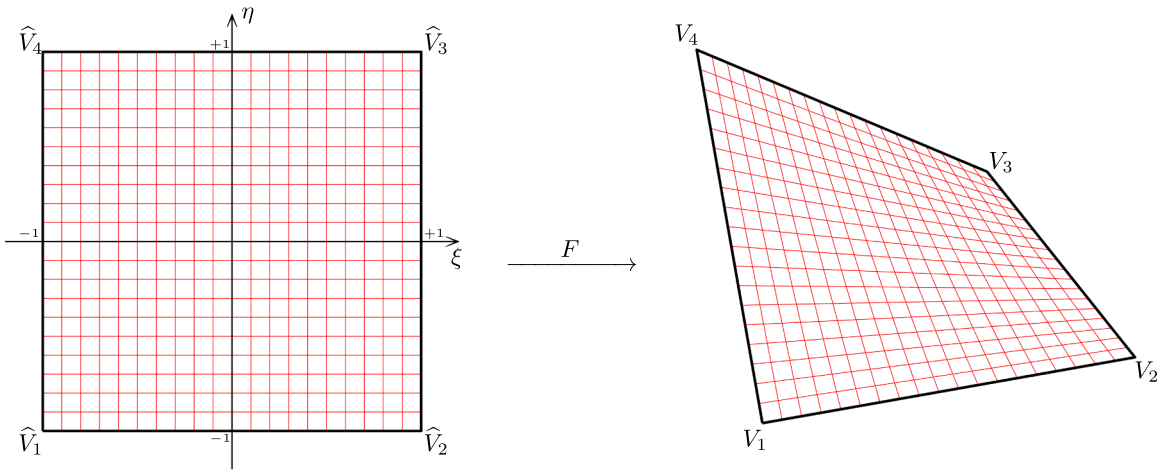

(a) Reference square $\widehat{\mathcal{Q}}$ (b) Quadrilateral $\mathcal{Q}$

Fig. 2. Convex $\mathcal{Q}$.

determinant of the Jacobian is positive at the four vertices to ensure that it is positive everywhere. In the next subsection, we describe in details the two-dimensional case, as it will be useful later.

For regular bricks $\mathcal{B}$ we have the classical $\mathbb{Q}_1$ isoparametric finite element, obtained by defining the basis function $N_i(x, y, z)$ as

$$N_i(x, y, z) := \widehat{N}_i(\xi, \eta, \zeta) \tag{4}$$

where $\mathbf{F}(\xi, \eta, \zeta) = (x, y, z)$ so that

$$\nabla_{(x,y,z)} N_i(x, y, z) = J_{\mathbf{F}}^{-\mathrm{T}}(x, y, z) \nabla_{(\xi,\eta,\zeta)} \widehat{N}_i(\xi, \eta, \zeta). \tag{5}$$

The stiffness matrix and load vector can be efficiently computed by integrating over the reference cube $\widehat{\mathcal{B}}$ using product Gaussian quadrature formulas.

2.1. Two-dimensional case

Let $\mathcal{Q} \subset \mathbb{R}^2$ be a quadrilateral with vertices $V_\alpha = (x_\alpha, y_\alpha)$, $\alpha = 1, \dots, 4$ and let $\widehat{\mathcal{Q}} = [-1, +1] \times [-1, +1]$ the reference biunit square.

Let $\widehat{V}_\alpha = (\xi_\alpha, \eta_\alpha)$ be the vertices of the reference square $\widehat{\mathcal{Q}}$, with $(\xi_1, \eta_1) = (-1, -1)$, $(\xi_2, \eta_2) = (+1, -1)$, $(\xi_3, \eta_3) = (+1, +1)$, $(\xi_4, \eta_4) = (-1, +1)$. The bilinear basis functions $\widehat{N}_\alpha(\xi, \eta)$ can be written as

$$\widehat{N}_\alpha(\xi, \eta) := \frac{1}{4}(1 + \xi_\alpha \xi)(1 + \eta_\alpha \eta). \tag{6}$$

The bilinear transformation map $F : \widehat{\mathcal{Q}} \to \mathbb{R}^2$ is then given by

$$F(\xi, \eta) = \sum_{\alpha=1}^{4} \widehat{N}_\alpha(\xi, \eta) V_\alpha. \tag{7}$$

If the quadrilateral $\mathcal{Q}$ is convex, the application F maps $\widehat{\mathcal{Q}}$ onto $\mathcal{Q}$ and is invertible, see Fig. 2.

If the quadrilateral $\mathcal{Q}$ is concave, the image of the reference square $\widehat{\mathcal{Q}}$ through the map F is *larger* than $\mathcal{Q}$; the rectangle $\widehat{\mathcal{R}}$ in Fig. 3a is mapped onto the region $\mathcal{R}$ of Fig. 3b which is outside $\mathcal{Q}$. The determinant of the Jacobian of the transformation F changes sign across the diagonal of $\widehat{\mathcal{R}}$, and each point in the region $\mathcal{R}$ of Fig. 3b maps back, through F, to two points in the rectangle $\widehat{\mathcal{R}}$ of Fig. 3b. The resulting points are symmetric across the diagonal.

3. The virtual brick

Consider a regular brick $\mathcal{B}$ which is the image through the map $\mathbf{F}$ of the reference cube $\widehat{\mathcal{B}}$. If we restrict the map $\mathbf{F}$ to a face of $\widehat{\mathcal{B}}$, by taking for instance $\zeta \equiv 1$, we obtain a bilinear map in (ξ, η) from the biunit square $[-1, +1]^2$ to a face $\mathtt{f}$ of $\mathcal{B}$, see Fig. 4.

We observe that the bilinear map $\mathbf{F}_{|\zeta \equiv 1}$ depends only on the vertices of the face $\mathtt{f}$, and can be expressed through the bilinear basis functions of the reference square in the same way as we did in Eq. (7). More precisely, given 4 points $V_\alpha^{\mathtt{f}}$, $\alpha = 1, \dots, 4$ in $\mathbb{R}^3$ which are the vertices of a face $\mathtt{f}$ of the brick $\mathcal{B}$, we define the bilinear map $\mathbf{F}^{\mathtt{f}} : \widehat{\mathcal{Q}} \to \mathbb{R}^3$ as

$$\mathbf{F}^{\mathtt{f}}(\xi, \eta) := \sum_{\alpha=1}^{4} \widehat{N}_\alpha(\xi, \eta) V_\alpha^{\mathtt{f}} \tag{8}$$

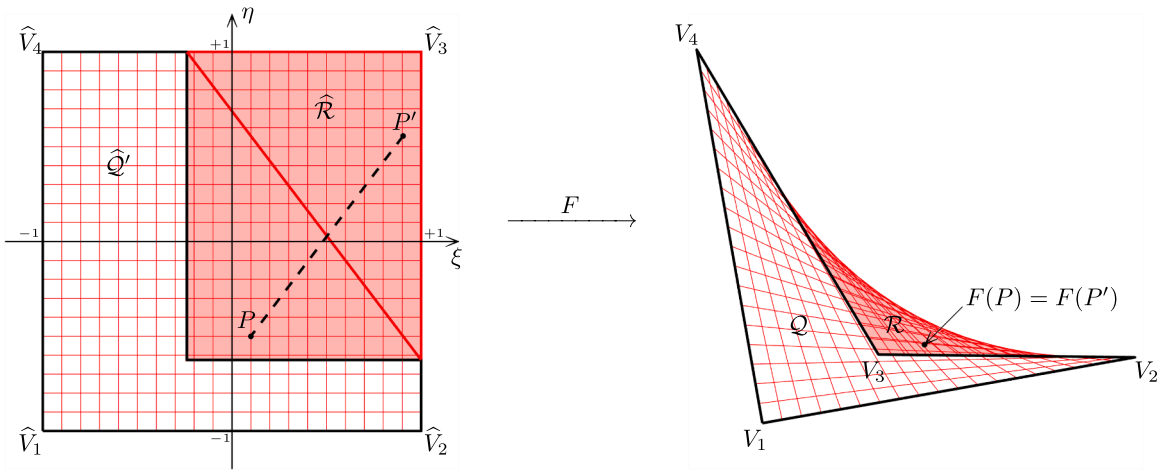

(a) Reference square $\widehat{\mathcal{Q}} = \widehat{\mathcal{Q}}' \cup \widehat{\mathcal{R}}$ (b) Quadrilateral $\mathcal{Q}$

Fig. 3. Concave $\mathcal{Q}$.

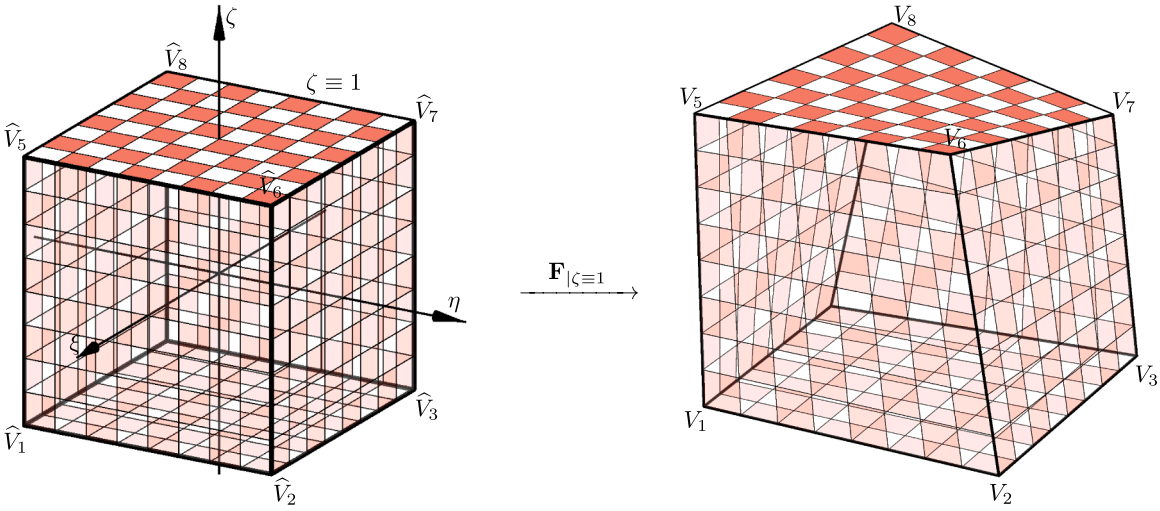

(a) Reference cube $\widehat{\mathcal{B}}$ (b) 8-node brick $\mathcal{B}$

Fig. 4. The bilinear face map $\mathbf{F}_{|\zeta\equiv 1}$.

where the function $\widehat{N}_\alpha$ are defined in (6). For each face $\mathtt{f}$, the map $\mathbf{F}^{\mathtt{f}}$ coincides with the restriction of the map $\mathbf{F}$ to the corresponding face of the reference cube $\widehat{\mathcal{B}}$, see Fig. 4. The resulting surface is a *hyperbolic paraboloid* (see Fig. 5).

If the brick is regular, the map $\mathbf{F}^{\mathtt{f}} : \widehat{\mathcal{Q}} \to \mathbf{F}^{\mathtt{f}}(\widehat{\mathcal{Q}})$ is invertible and $\mathtt{f} = \mathbf{F}^{\mathtt{f}}(\widehat{\mathcal{Q}})$. However, it can happen that the six maps $\mathbf{F}^{\mathtt{f}} : \widehat{\mathcal{Q}} \to \mathbf{F}^{\mathtt{f}}(\widehat{\mathcal{Q}})$ are invertible but the brick $\mathcal{B}$ is not regular. In Fig. 6b we show a non-regular brick obtained by starting from the reference cube $\widehat{\mathcal{B}}$ (see Fig. 1a) and then "pushing" vertices $\widehat{V}_1$ and $\widehat{V}_7$ towards the origin. In Fig. 6a we show the surfaces in the reference cube where the Jacobian is singular.

Definition 2. If the six functions $\mathbf{F}^{\mathtt{f}} : \widehat{\mathcal{Q}} \to \mathbf{F}^{\mathtt{f}}(\widehat{\mathcal{Q}})$ defined above are invertible and the faces do not intersect each other, we define the *virtual brick* $\mathcal{B}$ as the region of space enclosed by the union of all faces $\mathtt{f} = \mathbf{F}^{\mathtt{f}}(\widehat{\mathcal{Q}})$.

Remark 1. For a virtual brick, the map $\mathbf{F}$ is not necessarily invertible. When $\mathbf{F}$ is not invertible, the virtual brick $\mathcal{B}$ is no longer the image of the reference cube $\widehat{\mathcal{B}}$ through $\mathbf{F}$, since $\mathbf{F}(\widehat{\mathcal{B}})$ strictly contains $\mathcal{B}$. See Subsection 2.1 for a thorough analysis of the two-dimensional case.

Concerning the invertibility of the map $\mathbf{F}^{\mathtt{f}}$, we have the following theorem:

Theorem 1. *If the four vertices of* $\mathtt{f}$ *are not coplanar, then the map* $\mathbf{F}^{\mathtt{f}} : \widehat{\mathcal{Q}} \to \mathbf{F}^{\mathtt{f}}(\widehat{\mathcal{Q}})$ *is invertible. If the vertices are coplanar, the map* $\mathbf{F}^{\mathtt{f}}$ *is invertible if and only if they form a convex quadrilateral.*

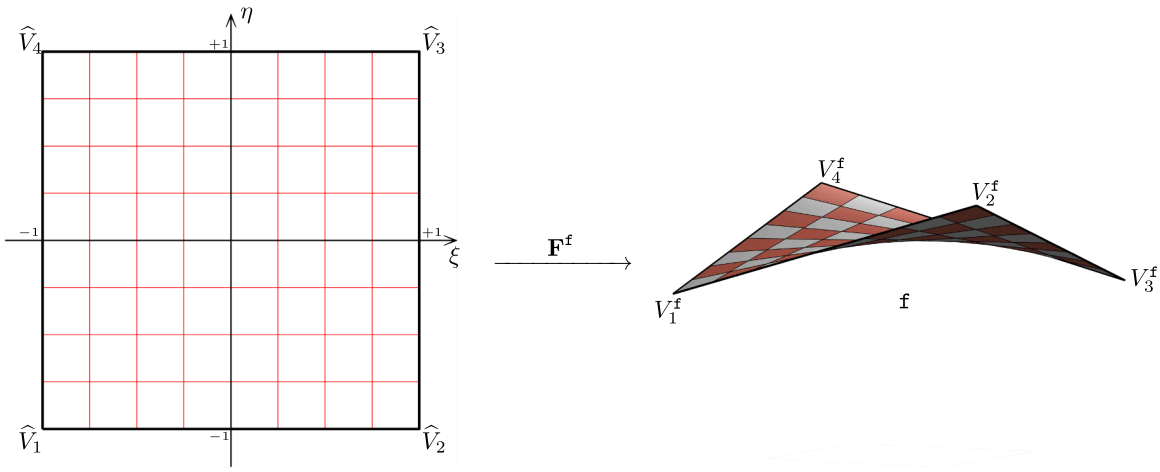

(a) Reference square $\widehat{\mathcal{Q}}$ (b) Face $\mathtt{f}$

Fig. 5. Mapped face.

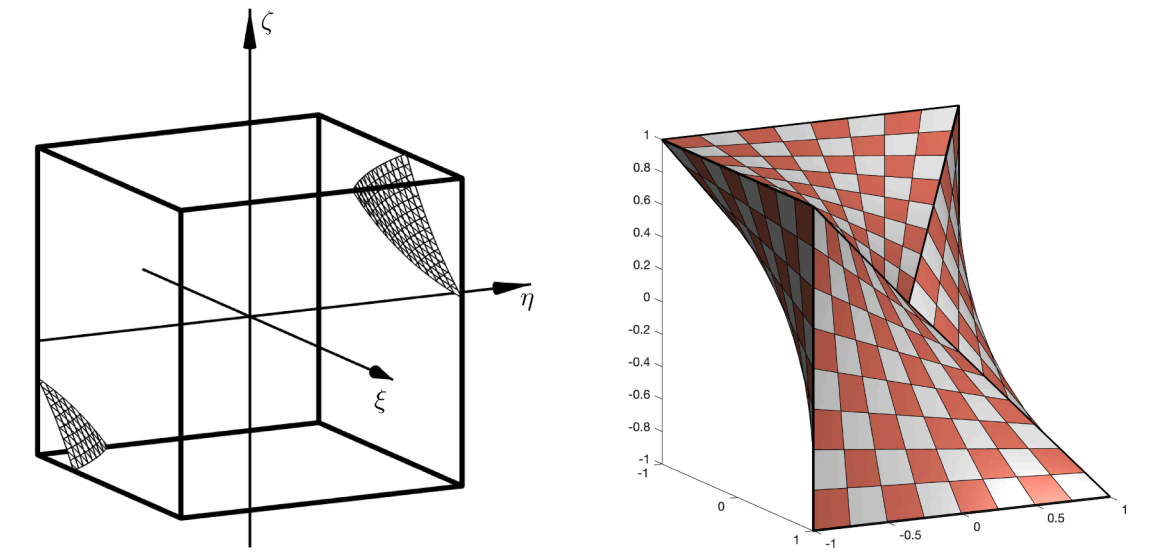

(a) Surface $\det J_{\mathbf{F}} = 0$ in $\widehat{\mathcal{B}}$ (b) Degenerate brick $\mathcal{B}$

Fig. 6. A degenerate brick.

Proof. Let $V_\alpha^{\mathtt{f}} = (x_\alpha, y_\alpha, z_\alpha)$, $\alpha = 1, \dots, 4$, and $\mathbf{F}^{\mathtt{f}} = (F_x^{\mathtt{f}}, F_y^{\mathtt{f}}, F_z^{\mathtt{f}})$. Then by (8)

$$F_x^{\mathtt{f}}(\xi,\eta) = \sum_{\alpha=1}^{4} \widehat{N}_\alpha(\xi,\eta)\, x_\alpha, \quad F_y^{\mathtt{f}}(\xi,\eta) = \sum_{\alpha=1}^{4} \widehat{N}_\alpha(\xi,\eta)\, y_\alpha, \quad F_z^{\mathtt{f}}(\xi,\eta) = \sum_{\alpha=1}^{4} \widehat{N}_\alpha(\xi,\eta)\, z_\alpha. \tag{9}$$

The functions $\widehat{N}_\alpha(\xi,\eta)$ are a set of barycentric coordinates, hence in particular the following identities hold:

$$1 = \sum_{\alpha=1}^{4} \widehat{N}_\alpha(\xi,\eta), \quad \xi = \sum_{\alpha=1}^{4} \xi_\alpha \widehat{N}_\alpha(\xi,\eta), \quad \eta = \sum_{\alpha=1}^{4} \eta_\alpha \widehat{N}_\alpha(\xi,\eta). \tag{10}$$

Let $\mathbf{P} = (P_x, P_y, P_z)$ be a point on $\mathtt{f} = \mathbf{F}^{\mathtt{f}}(\widehat{Q})$; we want to show that there is a unique (ξ, η) in $\widehat{Q}$ such that $\mathbf{F}^{\mathtt{f}}(\xi, \eta) = \mathbf{P}$. To this aim, we put together (9) and the first identity in (10), obtaining the linear relationship

$$\begin{bmatrix} 1 \\ P_x \\ P_y \\ P_z \end{bmatrix} = \begin{bmatrix} 1 & 1 & 1 & 1 \\ x_1 & x_2 & x_3 & x_4 \\ y_1 & y_2 & y_3 & y_4 \\ z_1 & z_2 & z_3 & z_4 \end{bmatrix} \begin{bmatrix} \widehat{N}_1(\xi, \eta) \\ \widehat{N}_2(\xi, \eta) \\ \widehat{N}_3(\xi, \eta) \\ \widehat{N}_4(\xi, \eta) \end{bmatrix}. \tag{11}$$

The matrix in (11) is invertible if and only if the four vertices V_i are not coplanar, since its determinant is the (signed) volume of the tetrahedron with vertices V_α multiplied by 6. Hence, if this is the case, we can invert (11) and recover $\widehat{N}_\alpha(\xi, \eta)$ in terms of $\mathbf{P}$. By expanding (10) together with the relation $\sum_{\alpha=1}^{4} (-1)^\alpha \widehat{N}_\alpha(\xi, \eta) = -\xi\eta$, we obtain

$$\begin{bmatrix} 1 \\ \xi \\ \eta \\ -\xi\eta \end{bmatrix} = \begin{bmatrix} +1 & +1 & +1 & +1 \\ -1 & +1 & +1 & -1 \\ -1 & -1 & +1 & +1 \\ -1 & +1 & -1 & +1 \end{bmatrix} \begin{bmatrix} \widehat{N}_1(\xi, \eta) \\ \widehat{N}_2(\xi, \eta) \\ \widehat{N}_3(\xi, \eta) \\ \widehat{N}_4(\xi, \eta) \end{bmatrix} \tag{12}$$

where the determinant of the matrix is $16 \neq 0$. Hence, if we start from a point $\mathbf{P} = (F_x^{\mathtt{f}}(\xi, \eta), F_y^{\mathtt{f}}(\xi, \eta), F_z^{\mathtt{f}}(\xi, \eta)) \in \mathtt{f}$ and the vertices of $\mathtt{f}$ are not coplanar, we get a unique $(\xi, \eta) \in \widehat{Q}$. Hence, the map $\mathbf{F}^{\mathtt{f}}$ is invertible.

If the vertices $V_\alpha^{\mathtt{f}}$ are coplanar, we can argue in the following way. We start by observing that if R is a rotation matrix in $\mathbb{R}^3$ and we rotate the vertices $V_\alpha^{\mathtt{f}}$ by multiplying them by R, the new map will simply be the old $\mathbf{F}^{\mathtt{f}}$ multiplied by R. Hence, if the vertices $V_\alpha^{\mathtt{f}}$ are coplanar, we can assume that they lie in the (x, y) plane. In this case, the map $\mathbf{F}^{\mathtt{f}}$ is the standard isoparametric map in $\mathbb{R}^2$ defined by (7), and, as we have already observed, it is invertible if and only if the four vertices form a convex quadrilateral. □

4. The virtual element space for the virtual brick

In this section, we construct a virtual element space $V_1^{\mathsf{VEM}}(\mathcal{B})$ on a virtual brick $\mathcal{B}$ that is face-compatible with the standard isoparametric finite element on regular bricks. We will only use the very basic ideas of the Virtual Element Method that can be found for instance in [12,38,39]. We follow the construction described in [39]: we first define an auxiliary space $\widetilde{V}_1^{\mathsf{VEM}}(\mathcal{B})$, then we construct the Π_1^∇ projector, and finally we define $V_1^{\mathsf{VEM}}(\mathcal{B})$ as a subspace of $\widetilde{V}_1^{\mathsf{VEM}}(\mathcal{B})$ by means of Π_1^∇. This construction will allow to compute, along with the Π_1^∇ projection, also the standard L^2 projection of virtual functions onto linear polynomials (see (22)), which is important to discretize zero-order terms (cf. the reaction term of (39), for instance).

Since we want our local space $\widetilde{V}_1^{\mathsf{VEM}}(\mathcal{B})$ to be face-compatible with the isoparametric brick, we begin by describing the face space $V_1^{\mathsf{ISO}}(\mathtt{f})$ of the 8-node isoparametric brick.

4.1. The face space $V_1^{ISO}(\mathtt{f})$

Let $\mathcal{B}$ be a regular brick. Then the local $\mathbb{Q}_1$ isoparametric space on $\mathcal{B}$ is defined through the trilinear map $\mathbf{F}$:

$$V_1^{\mathsf{ISO}}(\mathcal{B}) := \{v_h : \mathcal{B} \longrightarrow \mathbb{R} \text{ such that } v_h \circ \mathbf{F} \text{ is trilinear in } (\xi, \eta, \zeta)\}.$$

Let $\mathtt{f}$ be a face of $\mathcal{B}$. The space on $\mathtt{f}$ consists of the restrictions to $\mathtt{f}$ of functions in $V_1^{\mathsf{ISO}}(\mathcal{B})$; hence it is given by

$$V_1^{\mathsf{ISO}}(\mathtt{f}) = \{g_h : \mathtt{f} \to \mathbb{R} \text{ such that } g_h \circ \mathbf{F}^{\mathtt{f}} \text{ is bilinear in } (\xi, \eta)\}, \tag{13}$$

where we recall that the bilinear maps $\mathbf{F}^{\mathtt{f}}$ are obtained as restrictions of $\mathbf{F}$ to the faces of the reference cube $\widehat{\mathcal{B}}$ (see Fig. 4). We observe that the face space $V_1^{\mathsf{ISO}}(\mathtt{f})$ has dimension 4, and that a function $g_h \in V_1^{\mathsf{ISO}}(\mathtt{f})$ is completely determined by its value at the vertices of $\mathtt{f}$. In fact, given $g_h \in V_1^{\mathsf{ISO}}(\mathtt{f})$, since $g_h \circ \mathbf{F}^{\mathtt{f}}$ is bilinear it can be written as a linear combination of the basis $\widehat{N}_\alpha$ defined in (6):

$$g_h(\mathbf{F}^{\mathtt{f}}(\xi, \eta)) = \sum_{\alpha=1}^{4} c_\alpha \widehat{N}_\alpha(\xi, \eta)$$

and by taking $(\xi, \eta) = \widehat{V}_\beta$, we get $c_\beta = g_h(V_\beta^{\mathtt{f}})$. Hence we can define $V_1^{\mathsf{ISO}}(\mathtt{f})$ face by face even for a virtual brick, without needing to resort to the global map $\mathbf{F}$.

We show now that each isoparametric face space $V_1^{\mathsf{ISO}}(\mathtt{f})$ contains the restriction to $\mathtt{f}$ of linear polynomials. We have the following theorem:

Theorem 2. *Let $\mathtt{f}$ be a face of a virtual brick $\mathcal{B}$. Then:*

i) If the vertices of $\mathtt{f}$ are not coplanar, the space $V_1^{ISO}(\mathtt{f})$ consists precisely of the restrictions to $\mathtt{f}$ of linear polynomials.

ii) If the vertices of $\mathtt{f}$ are coplanar and form a convex quadrilateral, the space $V_1^{ISO}(\mathtt{f})$ contains strictly the restrictions to $\mathtt{f}$ of linear polynomials.

Proof. Let $p_1(x,y,z) = a + bx + cy + dz$ be a linear polynomial. Then with the notation of Theorem 1

$$(p_1 \circ \mathbf{F}^{\mathtt{f}})(\xi,\eta) = a + b\,F_x^{\mathtt{f}}(\xi,\eta) + c\,F_y^{\mathtt{f}}(\xi,\eta) + d\,F_z^{\mathtt{f}}(\xi,\eta)$$

which is obviously bilinear in (ξ,η). Hence, by (13), $p_{1|\mathtt{f}} \in V_1^{\mathsf{ISO}}(\mathtt{f})$, regardless of whether the vertices of $\mathtt{f}$ are coplanar or not.

i) As we have already observed, the dimension of $V_1^{\mathsf{ISO}}(\mathtt{f})$ is 4. Hence, to show that all functions in $V_1^{\mathsf{ISO}}(\mathtt{f})$ are restrictions to $\mathtt{f}$ of linear polynomials, it is enough to show that the restrictions to $\mathtt{f}$ of 1, x, y, and z are *linearly independent* in $V_1^{\mathsf{ISO}}(\mathtt{f})$. Since we have

$$1 \circ \mathbf{F}^{\mathtt{f}} = 1, \quad x \circ \mathbf{F}^{\mathtt{f}} = F_x^{\mathtt{f}}, \quad y \circ \mathbf{F}^{\mathtt{f}} = F_y^{\mathtt{f}}, \quad z \circ \mathbf{F}^{\mathtt{f}} = F_z^{\mathtt{f}}$$

and because $\mathbf{F}^{\mathtt{f}}$ is invertible by hypothesis, this is equivalent to showing that 1, $F_x^{\mathtt{f}}$, $F_y^{\mathtt{f}}$, and $F_z^{\mathtt{f}}$ are linearly independent on $\widehat{Q}$. From the proof of Theorem 1, we have the linear relationship

$$\begin{bmatrix} 1 \\ F_x^{\mathtt{f}} \\ F_y^{\mathtt{f}} \\ F_z^{\mathtt{f}} \end{bmatrix} = \begin{bmatrix} 1 & 1 & 1 & 1 \\ x_1 & x_2 & x_3 & x_4 \\ y_1 & y_2 & y_3 & y_4 \\ z_1 & z_2 & z_3 & z_4 \end{bmatrix} \begin{bmatrix} \widehat{N}_1 \\ \widehat{N}_2 \\ \widehat{N}_3 \\ \widehat{N}_4 \end{bmatrix} \tag{14}$$

where $V_\alpha^{\mathtt{f}} = (x_\alpha, y_\alpha, z_\alpha)$ are the vertices of the face $\mathtt{f}$. Since $\widehat{N}_1$, $\widehat{N}_2$, $\widehat{N}_3$, $\widehat{N}_4$ are linearly independent, the result follows if the matrix is nonsingular, which in turn is equivalent to the fact that the vertices of $\mathtt{f}$ are not coplanar.

ii) If the vertices of $\mathtt{f}$ are coplanar, the restriction to $\mathtt{f}$ of linear polynomials is the space of linear polynomials in two variables which has dimension 3; hence, since the dimension of $V_1^{\mathsf{ISO}}(\mathtt{f})$ is 4, it is strictly contained into it.

□

Since we want compatibility at the face level between the isoparametric brick and the virtual brick, we adopt definition (13) as the face space $V_1^{\mathsf{VEM}}(\mathtt{f})$ for functions on virtual bricks:

$$V_1^{\mathsf{VEM}}(\mathtt{f}) := V_1^{\mathsf{ISO}}(\mathtt{f}). \tag{15}$$

4.2. The auxiliary space $\widetilde{V}_1^{VEM}(\mathcal{B})$

We start defining the boundary space $B_1(\partial\mathcal{B})$ by gluing together with continuity the face spaces $V_1^{\mathsf{VEM}}(\mathtt{f})$:

$$B_1(\partial\mathcal{B}) := \{g_h : \partial\mathcal{B} \longrightarrow \mathbb{R} \text{ such that } g_h \in C^0(\partial\mathcal{B}) \text{ and } g_{h|\mathtt{f}} \in V_1^{\mathsf{VEM}}(\mathtt{f}) \text{ for all faces } \mathtt{f}\}.$$

The auxiliary VEM local space $\widetilde{V}_1^{\mathsf{VEM}}(\mathcal{B})$ is defined as the extension inside $\mathcal{B}$ through the Laplace operator of the boundary space $B_1(\partial\mathcal{B})$, i.e.

$$\widetilde{V}_1^{\mathsf{VEM}}(\mathcal{B}) := \{v_h : \mathcal{B} \longrightarrow \mathbb{R} \text{ such that } v_{h|\partial\mathcal{B}} \in B_1(\partial\mathcal{B}) \text{ and } \Delta v_h \in \mathbb{P}_1(x,y,z)\}. \tag{16}$$

The following Theorem characterizes the space $\widetilde{V}_1^{\mathsf{VEM}}(\mathcal{B})$:

Theorem 3. *The space $\widetilde{V}_1^{VEM}(\mathcal{B})$ has dimension $8+4=12$, and as degrees of freedom for $v_h \in \widetilde{V}_1^{VEM}(\mathcal{B})$ we can take:*

- *boundary degrees of freedom: the 8 pointwise values $v_h(V_i)$ at the vertices of $\mathcal{B}$, as for the isoparametric $\mathbb{Q}_1$ elements;*
- *internal degrees of freedom: the 4 moments against a basis for linear polynomials.*

Proof. For a bounded and sufficiently regular domain, the Dirichlet problem for the Laplace equation establishes a one-to-one linear correspondence between the boundary and source data and the solution; hence, since $\dim B_1(\partial\mathcal{B}) = 8$ and $\dim \mathbb{P}_1(x,y,z) = 4$, from the definition of $\widetilde{V}_1^{\mathsf{VEM}}(\mathcal{B})$ it is clear that $\dim \widetilde{V}_1^{\mathsf{VEM}}(\mathcal{B}) = 12$. To show that the pointwise values at the vertices and the moments of order up to one form a set of degrees of freedom for $\widetilde{V}_1^{\mathsf{VEM}}(\mathcal{B})$, is enough to show that

$$\left\{ v_h(V_i) = 0,\ i = 1,\dots,8 \quad \text{and} \quad \int_{\mathcal{B}} v_h\, p_1 \,\mathrm{d}\mathbf{x} = 0 \text{ for all } p_1 \in \mathbb{P}_1(x,y,z) \right\} \quad \text{implies} \quad v_h \equiv 0.$$

We first notice that since $v_h(V_i) = 0$, then $v_{h|\partial\mathcal{B}} = 0$. Integrating by parts $|v_h|^2_{1,\mathcal{B}}$, we have

$$|v_h|^2_{1,\mathcal{B}} = \int_{\mathcal{B}} |\nabla v_h|^2 \,\mathrm{d}\mathbf{x} = -\int_{\mathcal{B}} \Delta v_h\, v_h \,\mathrm{d}\mathbf{x} + \int_{\partial\mathcal{B}} \frac{\partial v_h}{\partial \mathbf{n}}\, v_h \,\mathrm{d}S.$$

The first term is zero because $\Delta v_h \in \mathbb{P}_1(x,y,z)$, while the second term is zero because $v_{h|\partial\mathcal{B}} = 0$. Hence $\nabla v_h \equiv 0$ so that v_h is constant, and being zero on $\partial\mathcal{B}$, it is zero everywhere. □

Remark 2. We have $\mathbb{P}_1(x,y,z) \subset \widetilde{V}_1^{\mathsf{VEM}}(\mathcal{B})$. In fact, by Theorem 2, $p_{1|\partial\mathcal{B}} \in B_1(\partial\mathcal{B})$ and $\Delta p_1 \equiv 0$.

4.3. The projector Π_1^∇

The next step in the definition of a Virtual Element Method is the computation of the projection Π_1^∇, which takes a function $v_h \in \widetilde{V}_1^{\mathsf{VEM}}(\mathcal{B})$ and projects it onto the space of linear polynomials $\mathbb{P}_1(x,y,z)$ using only its boundary degrees of freedom. The projection Π_1^∇ is defined by requiring that it is orthogonal with respect to the energy scalar product in $H_0^1(\mathcal{B})$, i.e.

$$\int_{\mathcal{B}} [\nabla \Pi_1^\nabla v_h] \cdot \nabla p_1 \, \mathrm{d}\mathbf{x} = \int_{\mathcal{B}} \nabla v_h \cdot \nabla p_1 \, \mathrm{d}\mathbf{x} \quad \text{for all } p_1 \in \mathbb{P}_1(x,y,z). \tag{17}$$

We need an extra condition to fix Π_1^∇ onto the constant functions. Here we will make use of the simplest possible choice, i.e.

$$\frac{1}{8}\sum_{i=1}^{8} [\Pi_1^\nabla v_h](V_i) = \frac{1}{8}\sum_{i=1}^{8} v_h(V_i); \tag{18}$$

we refer to [12] for the details. By observing that $\nabla[\Pi_1^\nabla v_h]$ is a constant vector, it is easy to see that (17) simply means that

$$\nabla[\Pi_1^\nabla v_h] = \frac{1}{\mathrm{vol}(\mathcal{B})} \int_{\mathcal{B}} \nabla v_h \, \mathrm{d}\mathbf{x} \tag{19}$$

and a direct application of (18) gives an explicit expression of $\Pi_1^\nabla v_h$:

$$[\Pi_1^\nabla v_h](\mathbf{x}) = \left[\frac{1}{\mathrm{vol}(\mathcal{B})} \int_{\mathcal{B}} \nabla v_h \, \mathrm{d}\mathbf{x}\right] \cdot (\mathbf{x} - \overline{V}) + \bar{v}_h \tag{20}$$

where $\overline{V} := \frac{1}{8}\sum_{i=1}^{8} V_i$ is the *vertex center* of $\mathcal{B}$ and $\bar{v}_h := \frac{1}{8}\sum_{i=1}^{8} v_h(V_i)$. The integral on $\mathcal{B}$ of the gradient of v_h can be explicitly computed given the boundary degrees of freedom of v_h, by

$$\int_{\mathcal{B}} \nabla v_h \, \mathrm{d}\mathbf{x} = \int_{\partial\mathcal{B}} v_h \mathbf{n} \, \mathrm{d}S = \sum_{\mathsf{f}} \left\{ \sum_{\alpha=1}^{4} v_h(V_\alpha^{\mathsf{f}}) \int_{\widehat{Q}} \widehat{N}_\alpha(\xi,\eta) \left(\frac{\partial \mathbf{F}^{\mathsf{f}}}{\partial \xi} \times \frac{\partial \mathbf{F}^{\mathsf{f}}}{\partial \eta} \right) \mathrm{d}\xi \, \mathrm{d}\eta \right\}.$$

We conclude that $\Pi_1^\nabla v_h$ depends only on the boundary degrees of freedom of v_h, and can be computed explicitly without recovering v_h inside $\mathcal{B}$.

Remark 3. By denoting with Π_0^0 the L^2 projection onto constants, by (19) we have

$$\nabla[\Pi_1^\nabla v_h] = \Pi_0^0[\nabla v_h]. \tag{21}$$

4.4. The space $V_1^{VEM}(\mathcal{B})$

We finally define $V_1^{\mathsf{VEM}}(\mathcal{B})$ as the subspace of $\widetilde{V}_1^{\mathsf{VEM}}(\mathcal{B})$ consisting of the virtual functions v_h whose moments against linear polynomials coincide with the corresponding moments of $\Pi_1^\nabla v_h$:

$$V_1^{\mathsf{VEM}}(\mathcal{B}) = \{ v_h \in \widetilde{V}_1^{\mathsf{VEM}}(\mathcal{B}) \text{ such that } \int_{\mathcal{B}} v_h \, p_1 \, \mathrm{d}\mathbf{x} = \int_{\mathcal{B}} \Pi_1^\nabla v_h \, p_1 \, \mathrm{d}\mathbf{x} \text{ for all } p_1 \in \mathbb{P}_1(x,y,z) \}.$$

Since $\int_{\mathcal{B}} v_h \, p_1 \, \mathrm{d}\mathbf{x} = \int_{\mathcal{B}} \Pi_1^0 v_h \, p_1 \, \mathrm{d}\mathbf{x}$, in $V_1^{\mathsf{VEM}}(\mathcal{B})$ we have the property

$$\Pi_1^0 v_h = \Pi_1^\nabla v_h \tag{22}$$

which allows us to compute the L^2 projection of virtual functions onto linear polynomials.

The next Theorem characterizes the space $V_1^{\mathsf{VEM}}(\mathcal{B})$.

Theorem 4. *The dimension of $V_1^{VEM}(\mathcal{B})$ is equal to 8 and as degrees of freedom in $V_1^{VEM}(\mathcal{B})$ we can take the boundary degrees of freedom of $\widetilde{V}_1^{VEM}(\mathcal{B})$, i.e. the pointwise values at the vertices of $\mathcal{B}$.*

Proof. Since $\dim \mathbb{P}_1(x,y,z) = 4$, the conditions defining $V_1^{\mathsf{VEM}}(\mathcal{B})$ as a subspace of $\widetilde{V}_1^{\mathsf{VEM}}(\mathcal{B})$ are 4, hence

$$\dim V_1^{\mathsf{VEM}}(\mathcal{B}) \geq \dim \widetilde{V}_1^{\mathsf{VEM}}(\mathcal{B}) - 4 = 8.$$

We prove that the dimension of $V_1^{\mathsf{VEM}}(\mathcal{B})$ is exactly 8 by showing that if the 8 boundary degrees of freedom of a function $v_h \in V_1^{\mathsf{VEM}}(\mathcal{B})$ are zero, then $v_h \equiv 0$. To this end, we just observe that if $v_h(V_i) = 0$, then $\Pi_1^\nabla v_h \equiv 0$, hence by (22) also $\Pi_1^0 v_h \equiv 0$ meaning that the internal degrees of freedom of v_h are zero as well. Hence by Theorem 3 we conclude that $v_h \equiv 0$.

Furthermore, it is clear from our argument that as degrees of freedom in the space $V_1^{\mathsf{VEM}}(\mathcal{B})$ we can take the boundary degrees of freedom of the space $\widetilde{V}_1^{\mathsf{VEM}}(\mathcal{B})$, i.e. the pointwise values at the vertices. □

The Lagrange basis functions $N_i(x,y,z) \in V_1^{\mathsf{VEM}}(\mathcal{B})$, $i = 1, \dots, 8$, are defined as usual by the condition $\mathrm{dof}_i(N_j) = N_j(V_i) = \delta_{ij}$.

Remark 4. We have $\mathbb{P}_1(x,y,z) \subsetneq V_1^{\mathsf{VEM}}(\mathcal{B})$. In fact, if $q_1 \in \mathbb{P}_1(x,y,z)$, we have $\Pi_1^\nabla q_1 = q_1$ so that the equation defining $V_1^{\mathsf{VEM}}(\mathcal{B})$ is trivially satisfied for $v_h = q_1$.

We summarize what we have done so far:

- given a virtual brick $\mathcal{B}$ (see Definition 2), we have defined the local virtual space $V_1^{\mathsf{VEM}}(\mathcal{B})$ (see (16)) which is an extension of the face spaces $V_1^{\mathsf{VEM}}(\mathtt{f}) = V_1^{\mathsf{ISO}}(\mathtt{f})$ glued together;
- the space $V_1^{\mathsf{VEM}}(\mathcal{B})$ has dimension 8 and contains linear polynomials. As degrees of freedom we take the pointwise values at the vertices;
- functions in $V_1^{\mathsf{VEM}}(\mathcal{B})$ are explicitly known (given the degrees of freedom) only on faces; however, as usual in the Virtual Element Method context, their values inside $\mathcal{B}$ are never used;
- if $\mathcal{B}$ is a virtual brick and $\mathcal{B}'$ is an adjacent regular brick, i.e. an isoparametric 8-node brick, the local space on their shared face is the same.

Remark 5. The previous construction can be repeated also for more general solids with both triangular and curved quadrilateral faces, opening the route to the construction of general polyhedral virtual elements featuring triangular faces and curved quadrilateral faces, suitable for the treatment of complex geometries.

Remark 6. The described virtual brick approach can be extended to the higher-order case. In fact, the face spaces can be defined by using the standard isoparametric design, while in the element interior one can follow the typical construction of the higher-order virtual elements.

5. Integration on a virtual brick

This section addresses the problem of integration over a virtual brick, with the goal of computing the stiffness matrix in practical applications.

We first consider functions that are known on the brick, and then turn to virtual functions, treated with a distinct approach.

5.1. Integration of monomials

On a virtual brick, monomials $x^\alpha y^\beta z^\gamma$ can be easily integrated by applying the divergence theorem. We choose for instance the x variable and observe that

$$x^\alpha y^\beta z^\gamma = \operatorname{div}\left(\frac{1}{\alpha+1} x^{\alpha+1} y^\beta z^\gamma \mathbf{e}_1\right) \tag{23}$$

where $\mathbf{e}_1 = (1,0,0)^T$. Hence,

$$\begin{aligned}\int_{\mathcal{B}} x^\alpha y^\beta z^\gamma \,\mathrm{d}\mathbf{x} &= \int_{\mathcal{B}} \operatorname{div}\left(\frac{1}{\alpha+1} x^{\alpha+1} y^\beta z^\gamma \mathbf{e}_1\right) \mathrm{d}\mathbf{x} = \\ &= \frac{1}{\alpha+1} \int_{\partial\mathcal{B}} x^{\alpha+1} y^\beta z^\gamma (\mathbf{e}_1 \cdot \mathbf{n}) \,\mathrm{d}S = \frac{1}{\alpha+1} \sum_{\mathtt{f}} \int_{\mathtt{f}} x^{\alpha+1} y^\beta z^\gamma (\mathbf{e}_1 \cdot \mathbf{n}^{\mathtt{f}}) \,\mathrm{d}S.\end{aligned} \tag{24}$$

The integral on each face $\mathtt{f}$ can be computed by going back to the reference square:

$$\int_{\mathtt{f}} x^{\alpha+1} y^\beta z^\gamma \left(\mathbf{e}_1 \cdot \mathbf{n}^{\mathtt{f}}\right) \mathrm{d}S = \int_{\widehat{Q}} F_x^{\mathtt{f}}(\xi,\eta)^{\alpha+1} F_y^{\mathtt{f}}(\xi,\eta)^\beta F_z^{\mathtt{f}}(\xi,\eta)^\gamma \left[\mathbf{e}_1 \cdot \left(\frac{\partial \mathbf{F}^{\mathtt{f}}}{\partial\xi} \times \frac{\partial \mathbf{F}^{\mathtt{f}}}{\partial\eta}\right)\right] \mathrm{d}\xi \,\mathrm{d}\eta, \tag{25}$$

where we have used that $\mathbf{n}\,\mathrm{d}S = \left(\frac{\partial \mathbf{F}^{\mathtt{f}}}{\partial\xi} \times \frac{\partial \mathbf{F}^{\mathtt{f}}}{\partial\eta}\right) \mathrm{d}\xi \,\mathrm{d}\eta$. By direct computation, it can be seen that the components of $\frac{\partial \mathbf{F}^{\mathtt{f}}}{\partial\xi} \times \frac{\partial \mathbf{F}^{\mathtt{f}}}{\partial\eta}$ are bilinear polynomials in ξ and η. Hence, the integrand in (25) has degree at most $(\alpha+1+\beta+\gamma)+1$ in each variable. Consequently, to compute the exact integral it is enough to take a $N \times N$ Gauss quadrature formula on the reference square where $N = \left\lceil \frac{\alpha+\beta+\gamma+3}{2} \right\rceil$.

5.2. Integration of general functions

We will present here a quadrature formula based on the use of the map from the reference cube, even in the case of a non-regular virtual brick $\mathcal{B}$ (i.e., when its geometry mapping is not invertible).

Given a function f defined on $\mathcal{B}$, if the trilinear map $\mathbf{F} : \widehat{\mathcal{B}} \to \mathcal{B}$ is invertible so that $\det J_{\mathbf{F}}(\boldsymbol{\xi}) > 0$, it is possible to compute $\int_{\mathcal{B}} f(\mathbf{x}) \,\mathrm{d}\mathbf{x}$ by using the change of variable determined by $\mathbf{F}$:

$$\int_{\mathcal{B}} f(\mathbf{x}) \,\mathrm{d}\mathbf{x} = \int_{\widehat{\mathcal{B}}} f(\mathbf{F}(\boldsymbol{\xi})) \det J_{\mathbf{F}}(\boldsymbol{\xi}) \,\mathrm{d}\boldsymbol{\xi}. \tag{26}$$

In this way we can readily evaluate numerically the integral on $\widehat{\mathcal{B}}$ by Gauss product quadrature formulas for the cube. Our claim is that formula (26) works also when $\mathcal{B}$ is not regular, despite the fact that $\mathbf{F}$ is no more invertible. Note that we take the determinant of the Jacobian of $\mathbf{F}$ with its sign.

We recall that for a non-regular virtual brick we have $\mathbf{F}(\widehat{\mathcal{B}}) \supsetneq \mathcal{B}$, i.e. the brick "folds". Hence, for the integral on the right hand side of (26) to make sense, we need to extend f to $\mathbf{F}(\widehat{\mathcal{B}}) \setminus \mathcal{B}$. We will see that the value of the integral is independent of the extension, as shown in the following theorem.

Theorem 5. *Let $f : \mathcal{B} \to \mathbb{R}$ be a continuous function, and let $\tilde{f}$ be a continuous extension of f defined on $\mathbf{F}(\widehat{\mathcal{B}}) \supseteq \mathcal{B}$. Then*

$$\int_{\mathcal{B}} f(\mathbf{x})\,\mathrm{d}\mathbf{x} = \int_{\widehat{\mathcal{B}}} \tilde{f}(\mathbf{F}(\boldsymbol{\xi}))\,\det J_{\mathbf{F}}(\boldsymbol{\xi})\,\mathrm{d}\boldsymbol{\xi}. \tag{27}$$

Proof. The proof of this result follows from a general theorem in geometric integration, which states that (27) holds whenever the map $\mathbf{F}$ has topological degree 1 (see, e.g., [40], Chap. 4; see also [41] for a very illuminating introduction to the subject). In our setting, this requirement is satisfied because, by Definition 2, the restriction of $\mathbf{F}$ to the boundary of $\widehat{\mathcal{B}}$ is an orientation-preserving bijection onto the boundary of $\mathcal{B}$. For completeness, we also provide below an elementary proof tailored to our specific case.

We start by proving Eq. (26) when f is a polynomial p. Let $\mathbf{P}$ be a polynomial vector field such that $\operatorname{div}\mathbf{P} = p$; for instance, we can take a primitive $\tilde{p}$ of p with respect to x and set $\mathbf{P} := (\tilde{p}, 0, 0)$. For any virtual brick $\mathcal{B}$, regular or not, by the divergence theorem we have

$$\int_{\mathcal{B}} p\,\mathrm{d}\mathbf{x} = \int_{\mathcal{B}} \operatorname{div}\mathbf{P}\,\mathrm{d}\mathbf{x} = \int_{\partial\mathcal{B}} \mathbf{P}\cdot\mathbf{n}\,\mathrm{d}S = \sum_{\mathrm{f}} \int_{\widehat{\mathcal{Q}}} \mathbf{P}(\mathbf{F}^{\mathrm{f}}(\xi,\eta)) \cdot \left(\frac{\partial \mathbf{F}^{\mathrm{f}}}{\partial \xi} \times \frac{\partial \mathbf{F}^{\mathrm{f}}}{\partial \eta}\right) \mathrm{d}\xi\,\mathrm{d}\eta. \tag{28}$$

If $\mathcal{B}$ is a regular brick, i.e. such that $\det J_{\mathbf{F}}(\boldsymbol{\xi}) > 0$ on $\widehat{\mathcal{B}}$, we also have

$$\int_{\mathcal{B}} p\,\mathrm{d}\mathbf{x} = \int_{\widehat{\mathcal{B}}} p(\mathbf{F}(\boldsymbol{\xi}))\,\det J_{\mathbf{F}}(\boldsymbol{\xi})\,\mathrm{d}\boldsymbol{\xi} \quad \text{(for } \mathcal{B} \text{ regular)}. \tag{29}$$

Consider now the two expressions above for $\int_{\mathcal{B}} p\,\mathrm{d}\mathbf{x}$ as functions of the coordinates of the vertices $(x_1, y_1, z_1, x_2, y_2, z_2, \dots)$ of the brick $\mathcal{B}$. Recall that both $\mathbf{F}$ and $\mathbf{F}^{\mathrm{f}}$ are a linear combination of vertices of $\mathcal{B}$ (see (3) and (8)). Thus, the 24 vertex coordinates appear in polynomial form in both integrands of (28) and (29), implying that, after integration, both expressions remain *polynomials* in these 24 variables.

To show that the two expressions (28) and (29) define the same polynomial, it suffices–by the identity theorem for multivariate polynomials–to verify that they agree on an open set in all variables. This condition is satisfied: if the brick $\mathcal{B}$ is regular (i.e., if its vertices are sufficiently close to those of the reference cube $\widehat{\mathcal{B}}$), then $\det J_{\mathbf{F}} > 0$ and the two expressions coincide. Since they agree on an open neighborhood of the vertex coordinates, they must be equal as polynomials, and thus coincide for *all* values of the vertex coordinates. In particular, they remain equal for any virtual brick $\mathcal{B}$, including the non-regular case.

Remark 7. Note that in the argument above it is not required that the map $\mathbf{F}^{\mathrm{f}}(\xi,\eta)$ be polynomial in ξ and η; the only property that actually matters is that $\mathbf{F}^{\mathrm{f}}(\xi,\eta)$ and $\mathbf{F}(\xi,\eta,\zeta)$ are linear combinations of the vertices V_i.

Let now $\tilde{f}$ be a continuous extension of f defined on $\mathbf{F}(\widehat{\mathcal{B}}) \supseteq \mathcal{B}$. By the Weierstrass theorem, for any $\varepsilon > 0$ there exists a polynomial p such that

$$\max_{\mathbf{x}\in\mathbf{F}(\widehat{\mathcal{B}})} |p(\mathbf{x}) - \tilde{f}(\mathbf{x})| < \varepsilon \tag{30}$$

so that

$$\begin{aligned}\left|\int_{\mathcal{B}} f\,\mathrm{d}\mathbf{x} - \int_{\widehat{\mathcal{B}}} \tilde{f}(\mathbf{F}(\boldsymbol{\xi}))\,\det J_{\mathbf{F}}(\boldsymbol{\xi})\,\mathrm{d}\boldsymbol{\xi}\right| \le{}& \left|\int_{\mathcal{B}} f\,\mathrm{d}\mathbf{x} - \int_{\mathcal{B}} p\,\mathrm{d}\mathbf{x}\right| + \left|\int_{\mathcal{B}} p\,\mathrm{d}\mathbf{x} - \int_{\widehat{\mathcal{B}}} p(\mathbf{F}(\boldsymbol{\xi}))\,\det J_{\mathbf{F}}(\boldsymbol{\xi})\,\mathrm{d}\boldsymbol{\xi}\right| \\ &+ \left|\int_{\widehat{\mathcal{B}}} p(\mathbf{F}(\boldsymbol{\xi}))\,\det J_{\mathbf{F}}(\boldsymbol{\xi})\,\mathrm{d}\boldsymbol{\xi} - \int_{\widehat{\mathcal{B}}} \tilde{f}(\mathbf{F}(\boldsymbol{\xi}))\,\det J_{\mathbf{F}}(\boldsymbol{\xi})\,\mathrm{d}\boldsymbol{\xi}\right|.\end{aligned} \tag{31}$$

The first and the third term can be bounded by a constant times ε, while the second term is zero. Hence the theorem is proved. □

An immediate consequence of this theorem is that

$$\int_{\mathbf{F}(\widehat{\mathcal{B}})\setminus\mathcal{B}} \tilde{f}\,\mathrm{d}\mathbf{x} = 0.$$

Hence, given a function f defined on $\mathcal{B}$, any continuous extension $\tilde{f}$ to $\mathbf{F}(\widehat{\mathcal{B}})$ leaves the integral computed via the isoparametric map unchanged; in other words, the exact integral does not depend on the choice of extension.

Remark 8. When the integral (27) is approximated using a quadrature formula, the result *does depend* on the extension $\tilde{f}$, because quadrature nodes that fall outside $\mathbf{F}(\widehat{\mathcal{B}})$ require evaluating $\tilde{f}$ at those points. Of course, if the extended function $\tilde{f}$ is smooth, accuracy is preserved.

When f is a polynomial, it is automatically defined on the whole $\mathbb{R}^3$. Hence a first important conclusion of this analysis is that *we can integrate polynomials on virtual bricks in the same way (i.e. with the same code) as on regular 8-node bricks.* As we have already observed, $\det J_{\mathbf{F}}(\xi,\eta,\zeta)$ is polynomial of maximum degree 2 in each variable; hence, to integrate exactly a polynomial $p_d(x,y,z)$ of degree d on $\mathcal{B}$ with formula (27), we need $N \times N \times N$ Gauss points on the reference cube where $N = \left\lceil \frac{d+3}{2} \right\rceil$:

$$\int_{\mathcal{B}} p_d(\mathbf{x})\,\mathrm{d}\mathbf{x} = \int_{\widehat{\mathcal{B}}} \underbrace{p_d(\mathbf{F}(\xi,\eta,\zeta))}_{\substack{\text{max degree } d \text{ in} \\ \text{each variable}}} \underbrace{\det J_{\mathbf{F}}(\xi,\eta,\zeta)}_{\substack{\text{max degree 2 in} \\ \text{each variable}}} \mathrm{d}\xi\,\mathrm{d}\eta\,\mathrm{d}\zeta. \tag{32}$$

Remark 9. From Remark 8, it emerges that the computation of volume integrals may require evaluating the integrand function at a Gauss quadrature point in the reference cubic element that is mapped to a point outside the physical domain of the distorted element. This is of particular concern in the case of nonsmooth material behavior, such as, e.g., elastoplasticity for solid mechanics problems. Theorem 5 states that the extension of the integrand function outside the element is arbitrary for the analytical value of the integral. Hence, a clever extrapolation of the integrand function using only the values inside the physical brick could give accurate results and this is the object of current investigations.

5.3. Integration of virtual functions

Virtual functions are known only through their degrees of freedom which in this case are the values at the vertices V_i of the virtual brick $\mathcal{B}$. It will be useful in the sequel to have at our disposal a quadrature formula which is exact for polynomials of degree 1 whose nodes are the vertices themselves. The quadrature formula will be based on least-squares approximation.

Let f be a function defined on $\mathcal{B}$, and let $p_1^{\mathrm{LS}} \in \mathbb{P}_1(x,y,z)$ the polynomial that approximates the value $f(V_i)$ in least-squares sense, i.e. such that

$$\sum_{i=1}^{8} \left| f(V_i) - p_1^{\mathrm{LS}}(V_i) \right|^2 \text{ is minimum.} \tag{33}$$

It is clear that such a polynomial exists and is unique unless all vertices of $\mathcal{B}$ are coplanar. Then we make the approximation

$$\int_{\mathcal{B}} f(\mathbf{x})\,\mathrm{d}\mathbf{x} \approx \int_{\mathcal{B}} p_1^{\mathrm{LS}}(\mathbf{x})\,\mathrm{d}\mathbf{x}. \tag{34}$$

If f belongs to $\mathbb{P}_1(x,y,z)$, then $p_1^{\mathrm{LS}} \equiv f$ so the quadrature formula has degree of precision at least 1. In order to identify the weights ω_i^{LS} of the quadrature formula constructed in this way, we define as π_i^{LS} the polynomial belonging to $\mathbb{P}_1(x,y,z)$ that approximates in the least square sense the data δ_{ij}, i.e.

$$\pi_i^{\mathrm{LS}}(V_i) \approx 1, \quad \pi_i^{\mathrm{LS}}(V_j) \approx 0 \quad \text{for } j \neq i. \tag{35}$$

Since the polynomial p_1^{LS} depends linearly on the data, we can express it as a linear combination of the polynomials $\pi_i^{\mathrm{LS}}(\mathbf{x})$ as follows:

$$p_1^{\mathrm{LS}}(\mathbf{x}) = \sum_{i=1}^{8} f(V_i)\,\pi_i^{\mathrm{LS}}(\mathbf{x}) \tag{36}$$

so that

$$\int_{\mathcal{B}} p_1^{\mathrm{LS}}(\mathbf{x})\,\mathrm{d}\mathbf{x} = \sum_{i=1}^{8} f(V_i) \int_{\mathcal{B}} \pi_i^{\mathrm{LS}}(\mathbf{x})\,\mathrm{d}\mathbf{x}. \tag{37}$$

Hence, the weights ω_i^{LS} of the quadrature formula are simply given by

$$\omega_i^{\mathrm{LS}} = \int_{\mathcal{B}} \pi_i^{\mathrm{LS}}\,\mathrm{d}\mathbf{x}. \tag{38}$$

6. VEM Approximation of a reaction-diffusion problem

For the sake of simplicity, we will consider the thermal problem with a reaction term, supplemented by Dirichlet boundary conditions:

$$\begin{cases} -\operatorname{div}(\mathsf{D}\nabla u) + cu = f & \text{in } \Omega \\ u = g & \text{on } \partial\Omega \end{cases} \tag{39}$$

where the diffusion $\mathsf{D} = \mathsf{D}(x,y,z)$ is a symmetric and uniformly positive definite 3×3 matrix and the reaction $c = c(x,y,z)$ is positive. The variational formulation of (39) reads

$$\begin{cases} \text{find } u \in H_g^1(\Omega), \text{ such that} \\ a(u,v) = F(v) \text{ for all } v \in H_0^1(\Omega) \end{cases} \tag{40}$$

where $H_g^1(\Omega) := \{v \in H^1(\Omega) \text{ such that } u = g \text{ on } \partial\Omega\}$ and

$$a(u,v) = \int_{\Omega} \left(\mathsf{D}\nabla u \cdot \nabla v + cuv\right)\mathrm{d}\mathbf{x}, \qquad F(v) = \int_{\Omega} f v\,\mathrm{d}\mathbf{x}. \tag{41}$$

Assume to subdivide Ω in virtual bricks $\mathcal{B}$ in a conformal way, and define the virtual spaces V_h and $V_{h,g}$ as

$$V_h = \{v \in H^1(\Omega) \text{ such that } v_{|\mathcal{B}} \in V_1^{\mathsf{VEM}}(\mathcal{B})\} \tag{42}$$

and

$$V_{h,g} = \{v \in V_h \text{ such that } v_{|\partial\Omega} = g_h\} \tag{43}$$

where on each boundary face $\mathtt{f}$, the function g_h is the interpolant of g at the vertices of $\mathtt{f}$. The approximate problem reads

$$\begin{cases} \text{find } u_h \in V_{h,g} \text{ such that} \\ a_h(u_h, v_h) = F_h(v_h) \text{ for all } v_h \in V_{h,0} \end{cases} \tag{44}$$

where $a_h(u_h, v_h)$ and $F_h(v_h)$ are written as

$$a_h(u_h, v_h) = \sum_{\mathcal{B}} a_h^{\mathcal{B}}(u_h, v_h), \quad F_h(v_h) = \sum_{\mathcal{B}} F_h^{\mathcal{B}}(v_h) \tag{45}$$

and $a_h^{\mathcal{B}}$, $F_h^{\mathcal{B}}$ are such that

$$a_h^{\mathcal{B}}(u_h, v_h) \approx \int_{\mathcal{B}} \left(\mathsf{D}\nabla u_h \cdot \nabla v_h + c u_h v_h\right) \mathrm{d}\mathbf{x} \quad \text{and} \quad F_h^{\mathcal{B}}(v_h) \approx \int_{\mathcal{B}} f v_h \, \mathrm{d}\mathbf{x}. \tag{46}$$

As standard in a finite element context, we have to compute for each brick $\mathcal{B}$ the local stiffness matrix $\mathsf{K}^{\mathcal{B}}$ and the load vector $\mathbf{b}^{\mathcal{B}}$:

$$\mathsf{K}_{ij}^{\mathcal{B}} := a_h^{\mathcal{B}}(N_j, N_i), \quad \mathbf{b}_i^{\mathcal{B}} := F_h^{\mathcal{B}}(N_i), \quad i, j = 1, \dots, 8.$$

6.1. Diffusion term

We start with the approximation of the diffusion term $\int_{\mathcal{B}} \mathsf{D}\nabla N_j \cdot \nabla N_i \, \mathrm{d}\mathbf{x}$. As standard in the Virtual Element Method, since the basis functions N_i are not known inside $\mathcal{B}$, we substitute them with their Π_1^∇ projections:

$$\int_{\mathcal{B}} \mathsf{D}\nabla N_j \cdot \nabla N_i \, \mathrm{d}\mathbf{x} \approx \int_{\mathcal{B}} \mathsf{D}\nabla[\Pi_1^\nabla N_j] \cdot \nabla[\Pi_1^\nabla N_i] \, \mathrm{d}\mathbf{x} = \int_{\mathcal{B}} \mathsf{D}\Pi_0^0[\nabla N_j] \cdot \Pi_0^0[\nabla N_i] \, \mathrm{d}\mathbf{x} \tag{47}$$

where the last equality follows from (20). The resulting matrix preserves consistency (see [12]) but it is rank-deficient. Indeed, to ensure the invertibility of the global stiffness matrix, its kernel should contain only the constant vector, hence its rank should be 7. However, since the image of the projector Π_0^0 has dimension 3, its rank is also 3. Hence, the matrix obtained by substituting ∇N_j with $\Pi_0^0[\nabla N_j]$ in the diffusion term needs to be supplemented with a stabilization matrix, which does not spoil consistency but restores the correct rank.

Remark 10. In view of Theorem 5, the integrals in (47) can be computed using the standard Gauss integration scheme of the isoparametric brick. This is of outmost importance in the case of nonlinear problems, where the material behaviour is usually evaluated at the Gauss points.

6.1.1. The dofi-dofi stabilization

A common choice (the so-called "dofi-dofi" stabilization; see [12] for a thorough discussion) is the following:

$$h_{\mathcal{B}} \frac{\mathrm{tr}\,(\mathsf{D}_{\mathcal{B}})}{3} \sum_{k=1}^{8} \mathrm{dof}_k(N_j - \Pi_1^\nabla N_j)\, \mathrm{dof}_k(N_i - \Pi_1^\nabla N_i), \tag{48}$$

where $\mathrm{dof}_k(v_h) := v_h(V_k)$ denotes the k-th degree of freedom of v_h, $h_{\mathcal{B}}$ is the diameter of $\mathcal{B}$, and $\mathsf{D}_{\mathcal{B}}$ is the value of D at the centroid of $\mathcal{B}$.

6.1.2. Self-Stabilized or stabilization free VEM

Following the approach proposed in [42], in Eq. (47) we could project ∇N_i onto a larger vector polynomial space, say $\mathbf{P}_\star(x, y, z)$, so that the resulting matrix

$$\int_{\mathcal{B}} \mathsf{D}\Pi_\star^0[\nabla N_j] \cdot \Pi_\star^0[\nabla N_i] \, \mathrm{d}\mathbf{x} \tag{49}$$

is no more rank-deficient and a stabilization term like (48) is no longer needed. To compute $\Pi_\star^0[\nabla v_h]$ directly from the degrees of freedom of v_h, the space $\mathbf{P}_\star$ should consist of divergence-free polynomials; in fact, computing $\Pi_\star^0[\nabla v_h]$ amounts to solve the linear problem

$$\int_{\mathcal{B}} \Pi_\star^0[\nabla v_h] \cdot \mathbf{q}_* \, \mathrm{d}\mathbf{x} = \int_{\mathcal{B}} \nabla v_h \cdot \mathbf{q}_* \, \mathrm{d}\mathbf{x} \quad \text{for all } \mathbf{q}_* \in \mathbf{P}_\star.$$

To evaluate the right-hand side, we integrate by parts:

$$\int_{\mathcal{B}} \nabla v_h \cdot \mathbf{q}_* \, \mathrm{d}\mathbf{x} = -\int_{\mathcal{B}} v_h \, \mathrm{div}\, \mathbf{q}_* \, \mathrm{d}\mathbf{x} + \int_{\partial\mathcal{B}} v_h \mathbf{q}_* \cdot \mathbf{n} \, \mathrm{d}S.$$

It is then clear that we need $\mathrm{div}\, \mathbf{q}_* = 0$ in order to eliminate the volume term, whose evaluation is impossible since v_h is unknown inside $\mathcal{B}$.

A natural candidate for a space of divergence-free polynomials $\mathbf{P}_\star$ is the space of gradients of harmonic polynomials of degree less than or equal to m:

$$\mathbf{P}_\star := \nabla \mathcal{H}_{\le m} = \{\nabla p_m^{\mathrm{H}}, \text{ with } p_m^{\mathrm{H}} \in \mathbb{P}_m(x, y, z) \text{ and } \Delta p_m^{\mathrm{H}} = 0\}.$$

The spaces $\nabla\mathcal{H}_{\leq m}$ are invariant under rigid motions, and, as a consequence, the matrix (49) is frame-indifferent. In the three-dimensional space, the dimension of $\nabla\mathcal{H}_{\leq m}$ is $(m+1)^2-1$ (see [43]).

• *Case* $m=2$. A necessary (but not sufficient) condition for the matrix (49) to have rank 7 is that $\dim(\mathbf{P}_\star)\geq 7$. When $m=2$, the dimension of $\nabla\mathcal{H}_{\leq 2}$ is $(2+1)^2-1=8$, so $\nabla\mathcal{H}_{\leq 2}$ is a potential candidate for $\mathbf{P}_\star$. However, it can be easily shown that in this case the rank of the matrix (49) is strictly less than 7 when $\mathcal{B}$ is a cube, for example. Indeed, let $\mathcal{B}$ be the reference cube $\widehat{\mathcal{B}}$ with vertices given by (1) and Ψ_h the virtual function defined by $\Psi_h(x,y,z)=xyz$. It is easy to check that Ψ_h takes the value $(-1)^i$ at vertex V_i for $i=1,2,3,4$, and $(-1)^{i+1}$ for $i=5,6,7,8$ so that, on each face, the values of Ψ_h at the vertices alternate between $+1$ and -1 and, as function of the parameters of the face, Ψ_h is given by $\pm\xi\eta$.

We show that $\Pi^0_\star[\nabla\Psi_h]=0$. In order to do so, we need to prove that for any $p_2^{\mathrm{H}}\in\mathcal{H}_{\leq 2}$, we have

$$\int_{\widehat{\mathcal{B}}}\nabla\Psi_h\cdot\nabla p_2^{\mathrm{H}}\,\mathrm{d}\mathbf{x}=0.$$

We integrate by parts:

$$\int_{\widehat{\mathcal{B}}}\nabla\Psi_h\cdot\nabla p_2^{\mathrm{H}}\,\mathrm{d}\mathbf{x}=-\int_{\widehat{\mathcal{B}}}\Psi_h\underbrace{\Delta p_2^{\mathrm{H}}}_{=0}\,\mathrm{d}\mathbf{x}+\sum_{\mathtt{f}}\int_{\mathtt{f}}\Psi_h\frac{\partial p_2^{\mathrm{H}}}{\partial\mathbf{n}}\,\mathrm{d}S=\sum_{\mathtt{f}}\int_{\mathtt{f}}\Psi_h\frac{\partial p_2^{\mathrm{H}}}{\partial\mathbf{n}}\,\mathrm{d}S,$$

because $\Delta p_2^{\mathrm{H}}\equiv 0$. Since $\widehat{\mathcal{B}}$ is the cube $[-1,+1]^3$, on each face in local coordinates (ξ,η) the virtual function Ψ_h is given by $\pm\xi\eta$ and $\dfrac{\partial p_2^{\mathrm{H}}}{\partial\mathbf{n}}$ is a first–order polynomial in ξ and η. Hence each integral reduces to the integration over the square $[-1,+1]^2$ of $\pm\xi\eta$ times a first–order polynomial in ξ and η, which yields always zero. As a consequence, the array $\Psi_h(V_i)$ is in the kernel of the matrix (49). In fact we have:

$$\sum_{j=1}^{8}\left[\int_{\widehat{\mathcal{B}}}\mathsf{D}\,\Pi^0_\star[\nabla N_j]\cdot\Pi^0_\star[\nabla N_i]\,\mathrm{d}\mathbf{x}\right]\Psi_h(V_j)=\int_{\widehat{\mathcal{B}}}\mathsf{D}\,\Pi^0_\star\nabla\left[\sum_{j=1}^{8}\Psi_h(V_j)N_j\right]\cdot\Pi^0_\star[\nabla N_i]\,\mathrm{d}\mathbf{x}=\int_{\widehat{\mathcal{B}}}\mathsf{D}\,\underbrace{\Pi^0_\star[\nabla\Psi_h]}_{=0}\cdot\Pi^0_\star[\nabla N_i]\,\mathrm{d}\mathbf{x}=0. \tag{50}$$

Hence the L^2 projection of $\nabla V_1^{\mathsf{VEM}}(\widehat{\mathcal{B}})$ into $\nabla\mathcal{H}_{\leq 2}$ is, in general, not sufficient to avoid the need for a stabilization term.

• *Case* $m=3$. When $m=3$, the dimension of $\mathbf{P}_\star=\nabla\mathcal{H}_{\leq 3}$ is $(3+1)^2-1=15$. In this case, for a cube the matrix (49) coincides with the stiffness matrix given by the $\mathbb{Q}_1$ isoparametric finite elements. Preliminary numerical experiments using this choice of $\mathbf{P}_\star$ yielded highly satisfactory results, which are reported in Section 8 together with the results obtained using the dofi-dofi stabilization (48).

For the actual computation, we list here a possible basis for the space $\nabla\mathcal{H}_{\leq 3}$, grouped by degree:

- degree 0:
$$\begin{bmatrix}1\\0\\0\end{bmatrix},\begin{bmatrix}0\\1\\0\end{bmatrix},\begin{bmatrix}0\\0\\1\end{bmatrix}$$

- degree 1:
$$\begin{bmatrix}0\\z\\y\end{bmatrix},\begin{bmatrix}-x\\2\,y\\-z\end{bmatrix},\begin{bmatrix}z\\0\\x\end{bmatrix},\begin{bmatrix}y\\x\\0\end{bmatrix},\begin{bmatrix}2\,x\\-y\\-z\end{bmatrix};$$

- degree 2:
$$\begin{bmatrix}2\,x\,z\\-8\,y\,z\\x^2-4\,y^2+3\,z^2\end{bmatrix},\begin{bmatrix}2\,x\,y\\x^2-2\,y^2+z^2\\2\,y\,z\end{bmatrix},\begin{bmatrix}3\,x^2-4\,y^2+z^2\\-8\,x\,y\\2\,x\,z\end{bmatrix},$$
$$\begin{bmatrix}-8\,x\,z\\2\,y\,z\\-4\,x^2+y^2+3\,z^2\end{bmatrix},\begin{bmatrix}-8\,x\,y\\-4\,x^2+3\,y^2+z^2\\2\,y\,z\end{bmatrix},\begin{bmatrix}-2\,x^2+y^2+z^2\\2\,x\,y\\2\,x\,z\end{bmatrix},\begin{bmatrix}y\,z\\x\,z\\x\,y\end{bmatrix}.$$

6.2. Reaction and load terms

The reaction and load terms appearing in the weak formulation of the problem can be approximated using different strategies.

- A first approach is to employ the quadrature formula described in Subsection 5.3. In this case, the integrals are replaced by discrete sums over the vertices of the element $\mathcal{B}$:
$$\int_{\mathcal{B}}c\,N_j N_i\,\mathrm{d}\mathbf{x}\approx\sum_{k=1}^{8}c(V_k)\,N_j(V_k)\,N_i(V_k)\,\omega_k^{\mathrm{LS}}=\sum_{k=1}^{8}c(V_k)\,\delta_{jk}\,\delta_{ik}\,\omega_k^{\mathrm{LS}}=\begin{cases}c(V_i)\,\omega_i^{\mathrm{LS}} & \text{if } i=j\\ 0 & \text{if } i\neq j\end{cases} \tag{51}$$

$$\int_{\mathcal{B}} f N_i \,\mathrm{d}\mathbf{x} \approx \sum_{k=1}^{8} f(V_k)\, N_i(V_k)\, \omega_k^{\mathrm{LS}} = \sum_{k=1}^{8} f(V_k)\, \delta_{ik}\, \omega_k^{\mathrm{LS}} = f(V_i)\, \omega_i^{\mathrm{LS}} \tag{52}$$

where the weights ω_k^{LS} are defined in (38).

- A second approach consists in substituting the basis functions N_i in the integrals with their L^2 projection $\Pi_1^0 N_i$ onto the space of linear polynomials (see Subsection 4.4, Eq. (22)), i.e.:

$$\int_{\mathcal{B}} c\, N_j N_i \,\mathrm{d}\mathbf{x} \approx \int_{\mathcal{B}} c\, (\Pi_1^0 N_j)\, (\Pi_1^0 N_i) \,\mathrm{d}\mathbf{x}, \qquad \int_{\mathcal{B}} f N_i \,\mathrm{d}\mathbf{x} \approx \int_{\mathcal{B}} f\, \Pi_1^0 N_i \,\mathrm{d}\mathbf{x}. \tag{53}$$

After this projection, the integrals can be computed using the method described in Subsection 5.2.

These two strategies provide consistent ways to evaluate the reaction and load contributions in the discrete formulation, depending on the computational framework used.

However, we remark that the second approach leads to a scheme for which a rigorous error analysis can be developed, see Section 7. For the first approach the same result could be established provided one were able to prove that the weights ω_k^{LS} are all positive. To our best knowledge, such a proof is not yet available for the vertex configuration of a general virtual brick. However, we highlight that all the numerical tests we have developed suggest that the weight positivity is true.

7. Convergence of the virtual brick method

In this Section we briefly consider the convergence property of the method described in Section 6. In particular, for the reaction term we select the approximation given by (53). Instead, for the loading term we can indifferently take one of the two choices (52) or (53). As usual, we introduce a sequence of brick meshes $\{\mathcal{T}_h\}_{h>0}$ with meshsize h. From now on, we denote by $h_{\mathcal{B}}$ the diameter of $\mathcal{B} \in \mathcal{T}_h$. For such a mesh sequence we assume what follows.

Hypotheses.

- **H1.** There exists $\rho > 0$, independent of h, such that every $\mathcal{B} \in \mathcal{T}_h$ is star-shaped with respect to a ball B_r, centered in $\mathbf{x}_0 \in \mathcal{B}$ and of radius r, with $\rho\, r \geq h_{\mathcal{B}}$ (of course, the radius r depend on $\mathcal{B}$; this dependence is here omitted for notational simplicity).
- **H2.** There exists $\gamma > 0$, independent of h, such that, given $\mathcal{B} \in \mathcal{T}_h$. it holds:
  - for every face $\mathtt{f}$ of $\mathcal{B}$, $\sqrt{\mathrm{Area}(\mathtt{f})} \geq \gamma\, h_{\mathcal{B}}$ (i.e. in a brick, the diameter of every face is comparable to the diameter of the brick itself);
  - for every edge e, $\mathrm{Length}(e) \geq \gamma\, h_{\mathcal{B}}$ (i.e. in a brick, the length of every edge is comparable to the diameter of the brick itself).
- **H3.** There exists σ, with $1 \geq \sigma > 0$ independent of h, such that, for every $\mathcal{B} \in \mathcal{T}_h$ and any vector $\mathbf{v} \in \mathbb{R}^3$, at least one vertex $V_j \in \mathcal{B}$ satisfies

$$(V_j - \mathbf{x}_0) \cdot \mathbf{v} \geq \sigma\, |V_j - \mathbf{x}_0|\, |\mathbf{v}| \quad (\mathbf{x}_0 \text{ as in } \mathbf{H1} \text{ above}). \tag{54}$$

Remark 11. We remark that assumptions **H1-H2** are on the line of the typical hypotheses assumed for the Virtual Element theoretical analysis. They are sufficient to define, for a regular analytical solution u of Problem (39), an interpolant u_I with optimal convergence rate properties. Assumption **H3** essentially means that the brick vertices are not *all* located in any half-space passing through $\mathbf{x}_0$. It is useful for the analysis of the first order least squares quadrature rule (see Section 7.1). We remark that such an assumption is satisfied in most of the meshes of practical interest.

Since the least squares approximation can be employed for the load term computation, we now consider the study of the resulting quadrature rules.

7.1. A first analysis of least squares quadrature rules

In this Section we focus on the quadrature rule (36)-(37), when using linear polynomials, as described in Section 5.3. Therefore, for a continuous function $\psi : \mathcal{B} \to \mathbb{R}$, we wish to study the error

$$\int_{\mathcal{B}} \psi(\mathbf{x}) \,\mathrm{d}\mathbf{x} - \int_{\mathcal{B}} p_1^{\mathrm{LS}}(\mathbf{x}) \,\mathrm{d}\mathbf{x} = \int_{\mathcal{B}} \psi(\mathbf{x}) \,\mathrm{d}\mathbf{x} - \sum_{i=1}^{8} \psi(V_i) \int_{\mathcal{B}} \pi_i^{\mathrm{LS}} \,\mathrm{d}\mathbf{x}. \tag{55}$$

We first prove the $L^\infty(\mathcal{B})$-stability of the construction $\psi \longrightarrow p_1^{\mathrm{LS}}$.

Theorem 6. *Under hypotheses* **H1** *and* **H3**, *for every* $\mathcal{B}$ *and every* $\psi \in L^\infty(\mathcal{B})$, *it holds*

$$||p_1^{LS}||_{L^\infty(\mathcal{B})} \lesssim ||\psi||_{L^\infty(\mathcal{B})}. \tag{56}$$

Proof. We notice that $p_1^{\mathrm{LS}} \in \mathbb{P}_1(\mathcal{B})$ is characterized by the following variational equations:

$$\sum_{i=1}^{8} p_1^{\mathrm{LS}}(V_i) q_1(V_i) = \sum_{i=1}^{8} \psi(V_i) q_1(V_i) \qquad \forall q_1 \in \mathbb{P}_1(\mathcal{B}). \tag{57}$$

Choosing $q_1 = p_1^{\mathrm{LS}}$, we get

$$\sum_{i=1}^{8} p_1^{\mathrm{LS}}(V_i)^2 \le \left(\sum_{i=1}^{8} \psi(V_i)^2\right)^{1/2} \left(\sum_{i=1}^{8} p_1^{\mathrm{LS}}(V_i)^2\right)^{1/2} \le 2\sqrt{2}||\psi||_{L^\infty(\mathcal{B})} \left(\sum_{i=1}^{8} p_1^{\mathrm{LS}}(V_i)^2\right)^{1/2}, \tag{58}$$

by which it holds

$$\left(\sum_{i=1}^{8} p_1^{\mathrm{LS}}(V_i)^2\right)^{1/2} \le 2\sqrt{2}||\psi||_{L^\infty(\mathcal{B})}. \tag{59}$$

Therefore, estimate (56) will follow if we prove that

$$||p_1^{\mathrm{LS}}||_{L^\infty(\mathcal{B})} \lesssim \left(\sum_{i=1}^{8} p_1^{\mathrm{LS}}(V_i)^2\right)^{1/2}. \tag{60}$$

We suppose $\nabla p_1^{\mathrm{LS}} \neq 0$, since (60) is trivial if p_1^{LS} is constant. We first remark that we have

$$||p_1^{\mathrm{LS}}||_{L^\infty(\mathcal{B})} \le \rho ||p_1^{\mathrm{LS}}||_{L^\infty(B_r)}. \tag{61}$$

We write $p_1^{\mathrm{LS}}(\mathbf{x})$ as $p_1^{\mathrm{LS}}(\mathbf{x}) = p_0 + \mathbf{a}\cdot(\mathbf{x}-\mathbf{x}_0)$, where $\mathbf{a}$ is (the constant vector) ∇p_1^{LS}. Hence, we have

$$||p_1^{\mathrm{LS}}||_{L^\infty(B_r)} = |p_0| + |\mathbf{a}|\, r = p_1^{\mathrm{LS}}(\mathbf{x}^*), \qquad \text{where } \mathbf{x}^* = \mathbf{x}_0 + \mathrm{sgn}(p_0)\, r\, \frac{\mathbf{a}}{|\mathbf{a}|}. \tag{62}$$

Due to assumption **H3**, taking $\mathbf{v} = \mathrm{sgn}(p_0)\,\mathbf{a}$, there exists a vertex $V_j \in \mathcal{B}$ that satisfies

$$(V_j - \mathbf{x}_0)\cdot(\mathrm{sgn}(p_0)\,\mathbf{a}) = |V_j - \mathbf{x}_0|\,|\mathbf{a}|\cos\vartheta_j \ge \sigma\,|V_j - \mathbf{x}_0|\,|\mathbf{a}|, \tag{63}$$

where ϑ_j denotes the angle formed by the vectors $V_j - \mathbf{x}_0$ and $\mathrm{sgn}(p_0)\,\mathbf{a}$. We notice that from (63) we have $\mathrm{sgn}[(V_j - \mathbf{x}_0)\cdot\mathbf{a}] = \mathrm{sgn}(p_0)$. Hence, still from (63) it holds:

$$\begin{aligned} |p_1^{\mathrm{LS}}(V_j)| &= |p_0 + \mathbf{a}\cdot(V_j - \mathbf{x}_0)| = |p_0\,\mathrm{sgn}(p_0) + (\mathrm{sgn}(p_0)\mathbf{a})\cdot(V_j - \mathbf{x}_0)| \\ &= |p_0| + |V_j - \mathbf{x}_0|\,|\mathbf{a}|\cos\vartheta_j \ge |p_0| + \sigma\,|V_j - \mathbf{x}_0|\,|\mathbf{a}| \ge |p_0| + \sigma\, r\,|\mathbf{a}| \\ &\ge \sigma\big(|p_0| + r\,|\mathbf{a}|\big) = \sigma||p_1^{\mathrm{LS}}||_{L^\infty(B_r)}. \end{aligned} \tag{64}$$

From (64) we thus get

$$||p_1^{\mathrm{LS}}||_{L^\infty(B_r)} \le \frac{1}{\sigma}\left(\sum_{i=1}^{8} p_1^{\mathrm{LS}}(V_i)^2\right)^{1/2}. \tag{65}$$

Combining (61) and (65) we get

$$||p_1^{\mathrm{LS}}||_{L^\infty(\mathcal{B})} \le \frac{\rho}{\sigma}\left(\sum_{i=1}^{8} p_1^{\mathrm{LS}}(V_i)^2\right)^{1/2}, \tag{66}$$

i.e. estimate (60). The proof is complete. □

A rough quadrature error estimation, but enough for our purposes, is detailed in the following result.

Theorem 7. *Under hypotheses* **H1** *and* **H3**, *consider a brick* $\mathcal{B}$. *Then for* $k = 0, 1, 2$ *it holds*

$$\left|\int_{\mathcal{B}} (\psi - p_1^{LS})\right| \lesssim \mathrm{vol}(\mathcal{B})\, h_{\mathcal{B}}^k |\psi|_{W^{k,\infty}(\mathcal{B})} \qquad \forall \psi \in W^{k,\infty}(\mathcal{B}). \tag{67}$$

Proof. We start by recalling that, by Stein's extension theorem (e.g., see [35]), given $\psi \in W^{k,\infty}(\mathcal{B})$ there exists an extension, for simplicity still denoted with ψ, such that

$$\psi \in W^{k,\infty}(\mathbb{R}^3) \qquad \text{and} \qquad ||\psi||_{W^{k,\infty}(\mathbb{R}^3)} \lesssim ||\psi||_{W^{k,\infty}(\mathcal{B})}. \tag{68}$$

We now denote by $C_{h_{\mathcal{B}}}$ a cube of diameter $\sqrt{3}\,h_{\mathcal{B}}$ such that $\mathcal{B} \subseteq C_{h_{\mathcal{B}}}$. From (68) we have

$$||\psi||_{W^{k,\infty}(C_{h_{\mathcal{B}}})} \lesssim ||\psi||_{W^{k,\infty}(\mathcal{B})}. \tag{69}$$

We remark that the application

$$\begin{aligned} L_1 \;:\; W^{k,\infty}(C_{h_{\mathcal{B}}}) &\longrightarrow \mathbb{P}_1(C_{h_{\mathcal{B}}}) \subset L^\infty(C_{h_{\mathcal{B}}}) \\ \psi &\mapsto L_1\psi := p_1^{\mathrm{LS}} \end{aligned} \tag{70}$$

is linear, continuous (by Theorem 6) and obviously $\mathbb{P}_1$-invariant. Exploiting the reference cube $\widehat{\mathcal{B}}$ we can thus invoke the Bramble-Hilbert lemma to obtain

$$||\psi - p_1^{\mathrm{LS}}||_{L^\infty(C_{h_{\mathcal{B}}})} \lesssim h_{\mathcal{B}}^k |\psi|_{W^{k,\infty}(C_{h_{\mathcal{B}}})}. \tag{71}$$

Hence, from Hölder inequality, estimates (71) and (69), we get

$$\begin{aligned}\left|\int_{\mathcal{B}}(\psi - p_1^{\mathrm{LS}})\right| &\le \int_{\mathcal{B}}|\psi - p_1^{\mathrm{LS}}| \le \mathrm{vol}(\mathcal{B})\,||\psi - p_1^{\mathrm{LS}}||_{L^\infty(\mathcal{B})} \\ &\le \mathrm{vol}(\mathcal{B})\,||\psi - p_1^{\mathrm{LS}}||_{L^\infty(C_{h_{\mathcal{B}}})} \lesssim \mathrm{vol}(\mathcal{B})\,h_{\mathcal{B}}^k|\psi|_{W^{k,\infty}(\mathcal{B})}\,.\end{aligned} \tag{72}$$

□

Summing all the local estimates of Theorem 7, for a mesh with size h we get the following global quadrature error bound.

Corollary 1. *Under hypotheses* **H1** *and* **H3**, *for* $k = 0, 1, 2$ *it holds*

$$\left|\int_{\Omega}(\psi - p_1^{LS})\right| \lesssim h^k\,\mathrm{vol}(\Omega)\,|\psi|_{W^{k,\infty}(\Omega)} \qquad \forall\psi \in W^{k,\infty}(\Omega)\,. \tag{73}$$

We now study the error stemming from the approximation of the load term, cf. (52). We have the following result.

Theorem 8. *Under hypotheses* **H1** *and* **H3**, *for every* $v_h \in V_h$ *and* $f \in W^{1,\infty}(\Omega)$, *it holds*

$$\int_{\Omega}(f v_h - L_1(f v_h)) \lesssim h||f||_{W^{1,\infty}(\Omega)}||v_h||_{1,\Omega}\,, \tag{74}$$

where L_1 *is defined by* (70).

Proof. We first establish local error bounds, on each brick $\mathcal{B}$. However, we need suitable modifications of the results described in Theorems 6 and 7. According to (57), the least squares approximation $L_1(f v_h) \in \mathbb{P}_1(\mathcal{B})$ is defined by

$$\sum_{i=1}^{8}[L_1(f v_h)](V_i)q_1(V_i) = \sum_{i=1}^{8} f(V_i)v_h(V_i)q_1(V_i) \qquad \forall q_1 \in \mathbb{P}_1(\mathcal{B}). \tag{75}$$

Choosing $q_1 = L_1(f v_h)$, we get

$$\begin{aligned}\sum_{i=1}^{8}[L_1(f v_h)](V_i)^2 &= \sum_{i=1}^{8} f(V_i)v_h(V_i)[L_1(f v_h)](V_i) \\ &\lesssim ||f||_{L^\infty(\mathcal{B})}\sum_{i=1}^{8} v_h(V_i)[L_1(f v_h)](V_i) \\ &\lesssim ||f||_{L^\infty(\mathcal{B})}\left(\sum_{i=1}^{8} v_h(V_i)^2\right)^{1/2}\left(\sum_{i=1}^{8}[L_1(f v_h)](V_i)^2\right)^{1/2}.\end{aligned} \tag{76}$$

We now notice that it holds

$$h_{\mathcal{B}}^{-1/2}(|v_h|_{H^1(\mathcal{B})} + h_{\mathcal{B}}^{-1}||v_h||_{L^2(\mathcal{B})}) \lesssim \left(\sum_{i=1}^{8} v_h(V_i)^2\right)^{1/2} \lesssim h_{\mathcal{B}}^{-1/2}(|v_h|_{H^1(\mathcal{B})} + h_{\mathcal{B}}^{-1}||v_h||_{L^2(\mathcal{B})})\,. \tag{77}$$

Hence, from (76) and (77) we have

$$\left(\sum_{i=1}^{8}[L_1(f v_h)](V_i)^2\right)^{1/2} \lesssim ||f||_{L^\infty(\mathcal{B})}\,h_{\mathcal{B}}^{-1/2}(|v_h|_{H^1(\mathcal{B})} + h_{\mathcal{B}}^{-1}||v_h||_{L^2(\mathcal{B})})\,. \tag{78}$$

Proceeding as in Theorem 6, we get

$$||L_1(f v_h)||_{L^\infty(\mathcal{B})} \lesssim ||f||_{L^\infty(\mathcal{B})}\,h_{\mathcal{B}}^{-1/2}(|v_h|_{H^1(\mathcal{B})} + h_{\mathcal{B}}^{-1}||v_h||_{L^2(\mathcal{B})})\,, \tag{79}$$

by which we also obtain

$$||L_1(f v_h)||_{L^2(\mathcal{B})} \lesssim \mathrm{vol}(\mathcal{B})^{1/2}\,||f||_{L^\infty(\mathcal{B})}\,h_{\mathcal{B}}^{-1/2}(|v_h|_{H^1(\mathcal{B})} + h_{\mathcal{B}}^{-1}||v_h||_{L^2(\mathcal{B})})\,. \tag{80}$$

In particular ($f = 1$), it holds

$$||L_1(v_h)||_{L^2(\mathcal{B})} \lesssim \mathrm{vol}(\mathcal{B})^{1/2}\,h_{\mathcal{B}}^{-1/2}(|v_h|_{H^1(\mathcal{B})} + h_{\mathcal{B}}^{-1}||v_h||_{L^2(\mathcal{B})})\,. \tag{81}$$

We denote with $\bar{f} \in \mathbb{P}_0(\mathcal{B})$ the mean value of $f_{|_{\mathcal{B}}}$ and write

$$\begin{aligned}\int_{\mathcal{B}}(f v_h - L_1(f v_h)) &= \int_{\mathcal{B}}\left(f v_h - L_1((f-\bar{f})v_h) - L_1(\bar{f}v_h)\right) \\ &= \int_{\mathcal{B}}\left((f-\bar{f})v_h - L_1((f-\bar{f})v_h) + \bar{f}v_h - L_1(\bar{f}v_h)\right) \\ &= \int_{\mathcal{B}}(f-\bar{f})v_h - \int_{\mathcal{B}} L_1((f-\bar{f})v_h) + \int_{\mathcal{B}}(\bar{f}v_h - L_1(\bar{f}v_h)) \\ &= T_1(\mathcal{B}) + T_2(\mathcal{B}) + T_3(\mathcal{B})\,.\end{aligned} \tag{82}$$

We separately bound the three terms above.
Bound for $T_1(\mathcal{B})$. A standard approximation result and Holdër and Cauchy-Schwarz inequalities give

$$T_1(\mathcal{B}) = \int_{\mathcal{B}} (f - \bar{f}) v_h \leq ||f - \bar{f}||_{L^\infty(\mathcal{B})} \int_{\mathcal{B}} |v_h| \lesssim |f|_{W^{1,\infty}(\mathcal{B})} h_{\mathcal{B}} \, \mathrm{vol}(\mathcal{B})^{1/2} ||v_h||_{L^2(\mathcal{B})} \, . \tag{83}$$

Bound for $T_2(\mathcal{B})$. From (79), Hölder inequality and standard approximation results, we obtain

$$\begin{aligned} T_2(\mathcal{B}) &= -\int_{\mathcal{B}} L_1((f - \bar{f}) v_h) \leq ||L_1((f - \bar{f}) v_h)||_{L^\infty(\mathcal{B})} \, \mathrm{vol}(\mathcal{B}) \\ &\leq ||f - \bar{f}||_{L^\infty(\mathcal{B})} \, \mathrm{vol}(\mathcal{B}) \, h_{\mathcal{B}}^{-1/2} (|v_h|_{H^1(\mathcal{B})} + h_{\mathcal{B}}^{-1} ||v_h||_{L^2(\mathcal{B})}) \\ &\lesssim |f|_{W^{1,\infty}(\mathcal{B})} \, \mathrm{vol}(\mathcal{B}) h_{\mathcal{B}}^{1/2} (|v_h|_{H^1(\mathcal{B})} + h_{\mathcal{B}}^{-1} ||v_h||_{L^2(\mathcal{B})}) \, . \end{aligned} \tag{84}$$

Bound for $T_3(\mathcal{B})$. Denoting with $\bar{v}_h$ the mean value of v_h over $\mathcal{B}$, noticing that it obviously holds $\bar{v}_h = L_1(\bar{v}_h)$, and using standard approximation results, we have

$$\begin{aligned} T_3(\mathcal{B}) &= \int_{\mathcal{B}} (\bar{f} v_h - L_1(\bar{f} v_h)) = \int_{\mathcal{B}} \bar{f} (v_h - L_1(v_h)) = \int_{\mathcal{B}} \bar{f} ((v_h - \bar{v}_h) - L_1(v_h - \bar{v}_h)) \\ &\leq ||f||_{L^\infty(\mathcal{B})} \int_{\mathcal{B}} (|v_h - \bar{v}_h| + |L_1(v_h - \bar{v}_h)|) \\ &\leq ||f||_{L^\infty(\mathcal{B})} \, \mathrm{vol}(\mathcal{B})^{1/2} \left(||v_h - \bar{v}_h||_{L^2(\mathcal{B})} + ||L_1(v_h - \bar{v}_h)||_{L^2(\mathcal{B})} \right) \\ &\lesssim ||f||_{L^\infty(\mathcal{B})} \, \mathrm{vol}(\mathcal{B})^{1/2} \left(h_{\mathcal{B}} |v_h|_{H^1(\mathcal{B})} + ||L_1(v_h - \bar{v}_h)||_{L^2(\mathcal{B})} \right) \, . \end{aligned} \tag{85}$$

We now exploit estimate (81) and a Poincaré-Wirtinger inequality for the $v_h - \bar{v}_h$, to get

$$T_3(\mathcal{B}) \lesssim ||f||_{L^\infty(\mathcal{B})} \, \mathrm{vol}(\mathcal{B})^{1/2} \left(h_{\mathcal{B}} |v_h|_{H^1(\mathcal{B})} + \mathrm{vol}(\mathcal{B})^{1/2} \, h_{\mathcal{B}}^{-1/2} |v_h|_{H^1(\mathcal{B})} \right) \, . \tag{86}$$

We are now ready to estimate $\int_\Omega (f v_h - L_1(f v_h))$ by summing all the local contributions. From (82), (83), (84) and (86), noticing that $\mathrm{vol}(\mathcal{B}) \approx h_{\mathcal{B}}^3$, we get

$$\begin{aligned} \int_\Omega (f v_h - L_1(f v_h)) &= \sum_{\mathcal{B}} \left(T_1(\mathcal{B}) + T_2(\mathcal{B}) + T_3(\mathcal{B}) \right) \\ &\lesssim \sum_{\mathcal{B}} ||f||_{W^{1,\infty}(\mathcal{B})} \mathrm{vol}(\mathcal{B})^{1/2} \, h_{\mathcal{B}} \, ||v_h||_{H^1(\mathcal{B})} \\ &\leq h \, ||f||_{W^{1,\infty}(\Omega)} \sum_{\mathcal{B}} \mathrm{vol}(\mathcal{B})^{1/2} \, ||v_h||_{H^1(\mathcal{B})} \\ &\leq h \, ||f||_{W^{1,\infty}(\Omega)} \left(\sum_{\mathcal{B}} \mathrm{vol}(\mathcal{B}) \right)^{1/2} \left(\sum_{\mathcal{B}} ||v_h||^2_{H^1(\mathcal{B})} \right)^{1/2} \\ &= h \, ||f||_{W^{1,\infty}(\Omega)} \, \mathrm{vol}(\Omega)^{1/2} \, ||v_h||_{H^1(\Omega)} \, , \end{aligned} \tag{87}$$

i.e. estimate (74). □

7.2. Statement of the convergence results

We conclude this Section by stating the convergence Theorems of our method. We recall that the reaction term $\int_\Omega cuv$ is approximated by using the local L^2 projection onto the linear polynomials, cf. (53). Instead, the load term $\int_\Omega fv$ can be treated using the local least squares approach, cf. (52), or alternatively the local L^2 projection onto the linear polynomials, again cf. (53).

7.2.1. Load term computed by means of the L^2 projection

For this case it is possible to prove the following optimal convergence result, whose proof is omitted since it can be developed using standard techniques (see [12], for example).

Theorem 9. *Let u be the solution of Problem (39) and $u_h \in V_h$ be the solution of Problem (44). Suppose that hypotheses* **H1** *and* **H2** *are fulfilled, and $u \in H^1_g(\Omega) \cap H^2(\Omega)$. Then it holds:*

$$||u - u_h||_{H^1(\Omega)} = O(h) \, . \tag{88}$$

7.2.2. Load term computed by means of least squares approximation

For this case it is still possible to prove an optimal convergence result:

Theorem 10. *Let u be the solution of Problem (39) and $u_h \in V_h$ be the solution of Problem (44). Suppose that hypotheses* **H1**, **H2** *and* **H3** *are fulfilled, and $u \in H^1_g(\Omega) \cap H^2(\Omega)$. Then it holds:*

$$||u - u_h||_{H^1(\Omega)} = O(h) \, . \tag{89}$$

Table 1
Description of the six numerical schemes used in the numerical tests shown in Figures 9–14, which investigate the effect of increasing distortion parameter d.

label	method	line style
ISO 2×2×2:	$\mathbb{Q}_1$ isoparametric FEM, 2×2×2 Gauss points	solid green (◇)
ISO 4×4×4:	$\mathbb{Q}_1$ isoparametric FEM, 4×4×4 Gauss points	dashed green (◇)
VEM:	dofi-dofi stabilized VEM for all bricks	solid blue (∗)
SSVEM:	Self-Stabilized VEM for all bricks	solid red (∗)
ISO-VEM:	•$\mathbb{Q}_1$ isoparametric FEM for regular bricks •dofi-dofi stabilized VEM for degenerate bricks	dashed blue (○)
ISO-SSVEM:	•$\mathbb{Q}_1$ isoparametric FEM for regular bricks •Self-Stabilized VEM for degenerate bricks	dashed red (○)

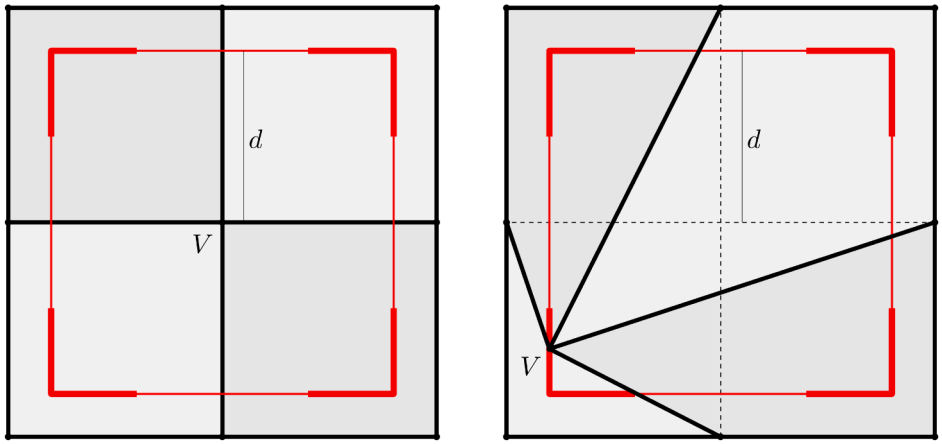

Fig. 7. Displacement of the central vertex V of a 2×2 block according to the distortion parameter d.

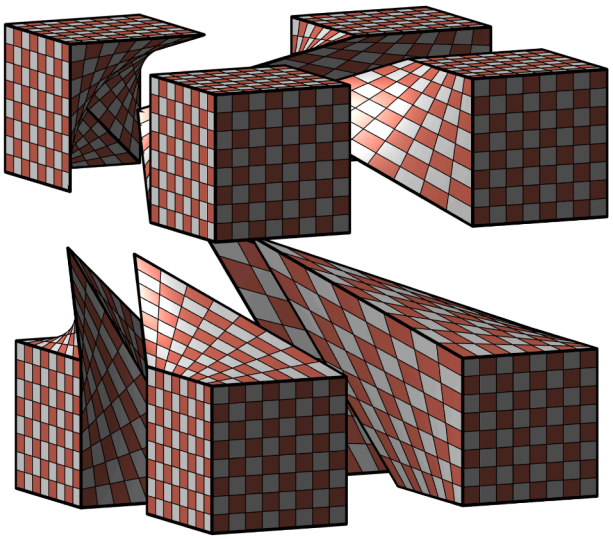

Fig. 8. Example of the distorsion of a $2 \times 2 \times 2$ block of bricks.

Again, the proof is omitted as it follows standard guidelines. However, we observe that from Theorem 8 we obviously get

$$\sup_{v_h \in V_h} \frac{\int_\Omega (f v_h - L_1(f v_h))}{||v_h||_{1,\Omega}} \lesssim h ||f||_{W^{1,\infty}(\Omega)} \,. \tag{90}$$

This means, by the first Strang lemma, that the load computation using the least squares approximation under consideration, does not affect the first order convergence rate of the method.

$d=0$				
N	# regular bricks	# degen. bricks	**(2)**	**(4)**
4	64 (100.0%)	0 (0.0%)	0	0
6	216 (100.0%)	0 (0.0%)	0	0
8	512 (100.0%)	0 (0.0%)	0	0
12	1728 (100.0%)	0 (0.0%)	0	0
16	4096 (100.0%)	0 (0.0%)	0	0
24	13824 (100.0%)	0 (0.0%)	0	0

(2): det $J_{\mathbf{F}} < 0$ at some $2\times2\times2$ Gauss quadrature points.
(4): det $J_{\mathbf{F}} < 0$ at some $4\times4\times4$ Gauss quadrature points.

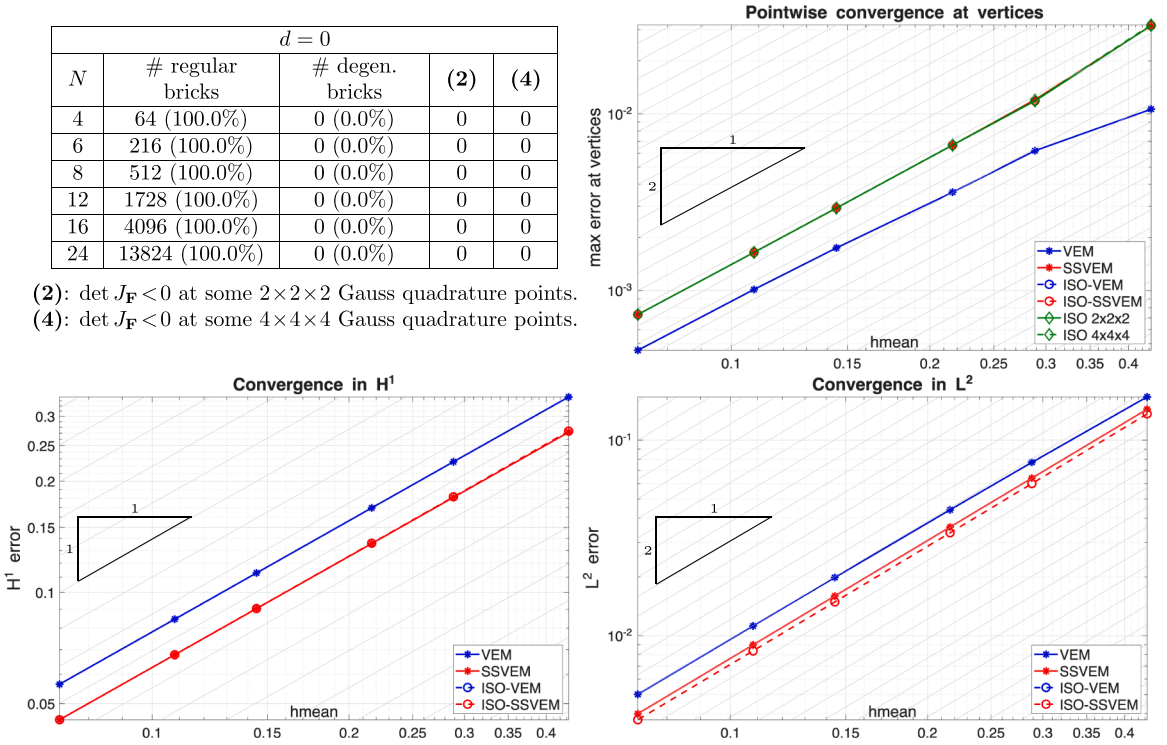

Fig. 9. Distortion $d = 0$.

$d=0.2$				
N	# regular bricks	# degen. bricks	**(2)**	**(4)**
4	64 (100.0%)	0 (0.0%)	0	0
6	216 (100.0%)	0 (0.0%)	0	0
8	512 (100.0%)	0 (0.0%)	0	0
12	1728 (100.0%)	0 (0.0%)	0	0
16	4096 (100.0%)	0 (0.0%)	0	0
24	13824 (100.0%)	0 (0.0%)	0	0

(2): det $J_{\mathbf{F}} < 0$ at some $2\times2\times2$ Gauss quadrature points.
(4): det $J_{\mathbf{F}} < 0$ at some $4\times4\times4$ Gauss quadrature points.

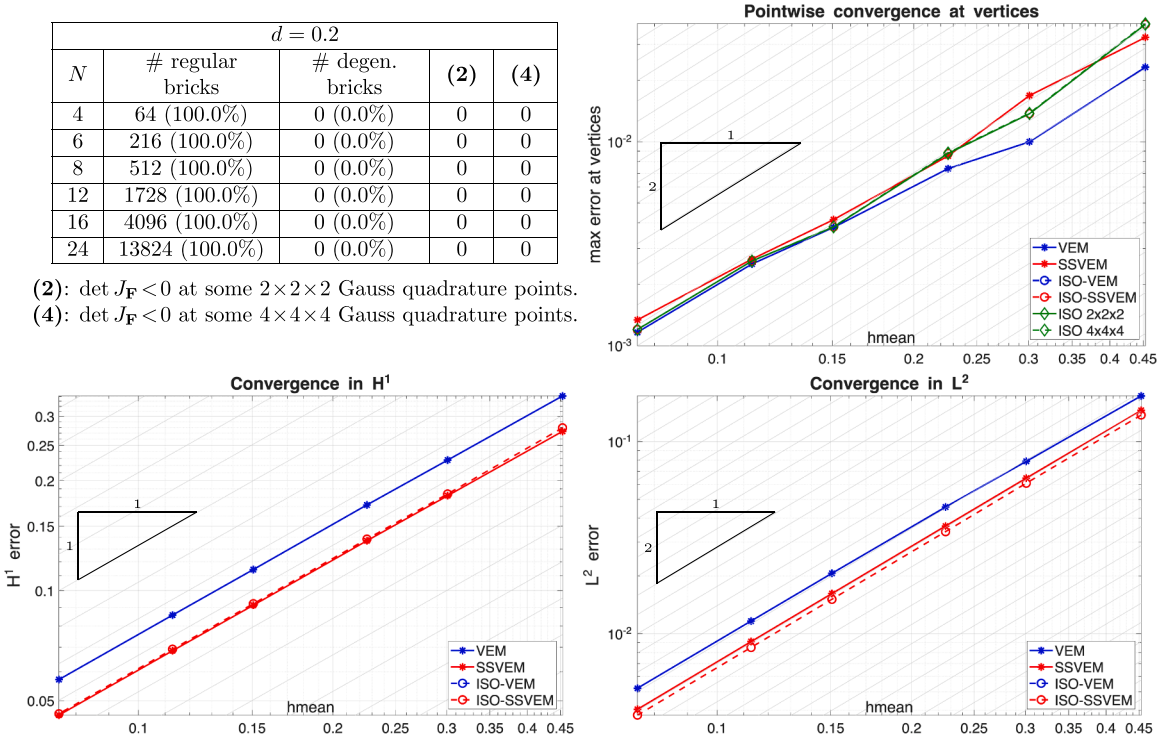

Fig. 10. Distortion $d = 0.2$.

$d = 0.4$				
N	# regular bricks	# degen. bricks	**(2)**	**(4)**
4	59 (92.2%)	5 (7.8%)	0	1
6	211 (97.7%)	5 (2.3%)	0	0
8	498 (97.3%)	14 (2.7%)	0	1
12	1671 (96.7%)	57 (3.3%)	0	3
16	3981 (97.2%)	115 (2.8%)	0	8
24	13397 (96.9%)	427 (3.1%)	0	17

(2): det $J_{\mathbf{F}} < 0$ at some $2\times2\times2$ Gauss quadrature points.
(4): det $J_{\mathbf{F}} < 0$ at some $4\times4\times4$ Gauss quadrature points.

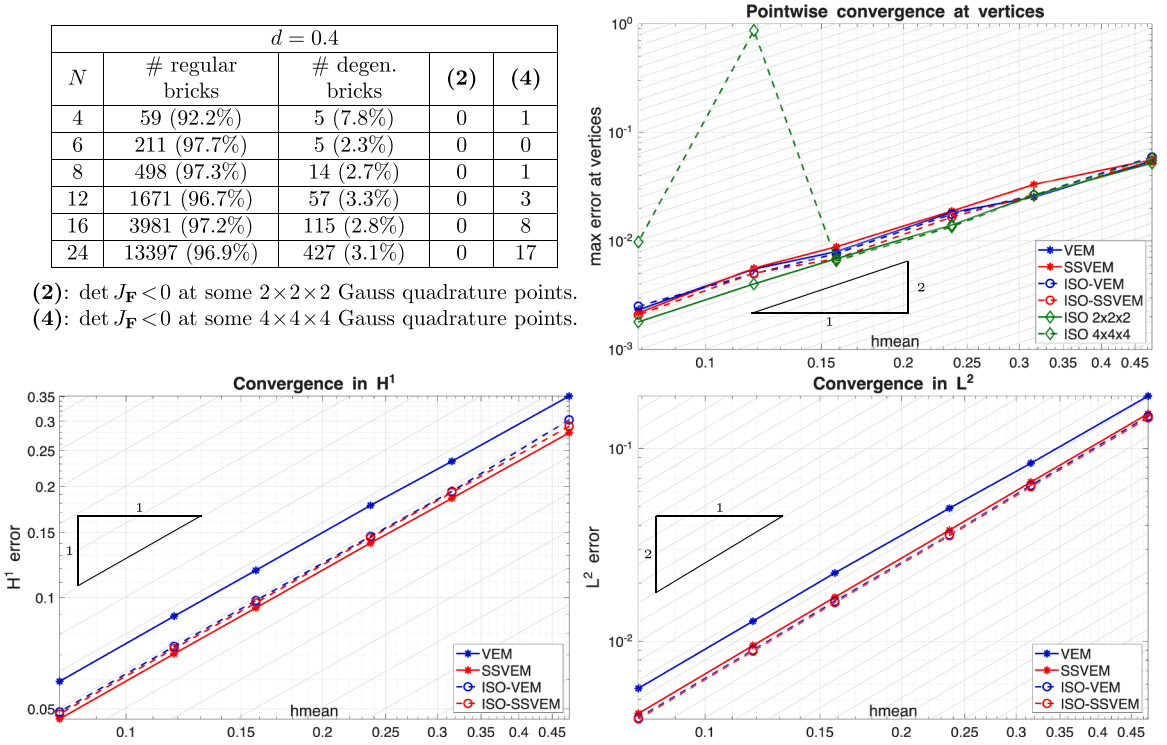

Fig. 11. Distortion $d = 0.4$.

$d = 0.6$				
N	# regular bricks	# degen. bricks	**(2)**	**(4)**
4	56 (87.5%)	8 (12.5%)	4	8
6	189 (87.5%)	27 (12.5%)	0	26
8	448 (87.5%)	64 (12.5%)	2	60
12	1512 (87.5%)	216 (12.5%)	17	211
16	3584 (87.5%)	512 (12.5%)	39	493
24	12096 (87.5%)	1728 (12.5%)	152	1667

(2): det $J_{\mathbf{F}} < 0$ at some $2\times2\times2$ Gauss quadrature points.
(4): det $J_{\mathbf{F}} < 0$ at some $4\times4\times4$ Gauss quadrature points.

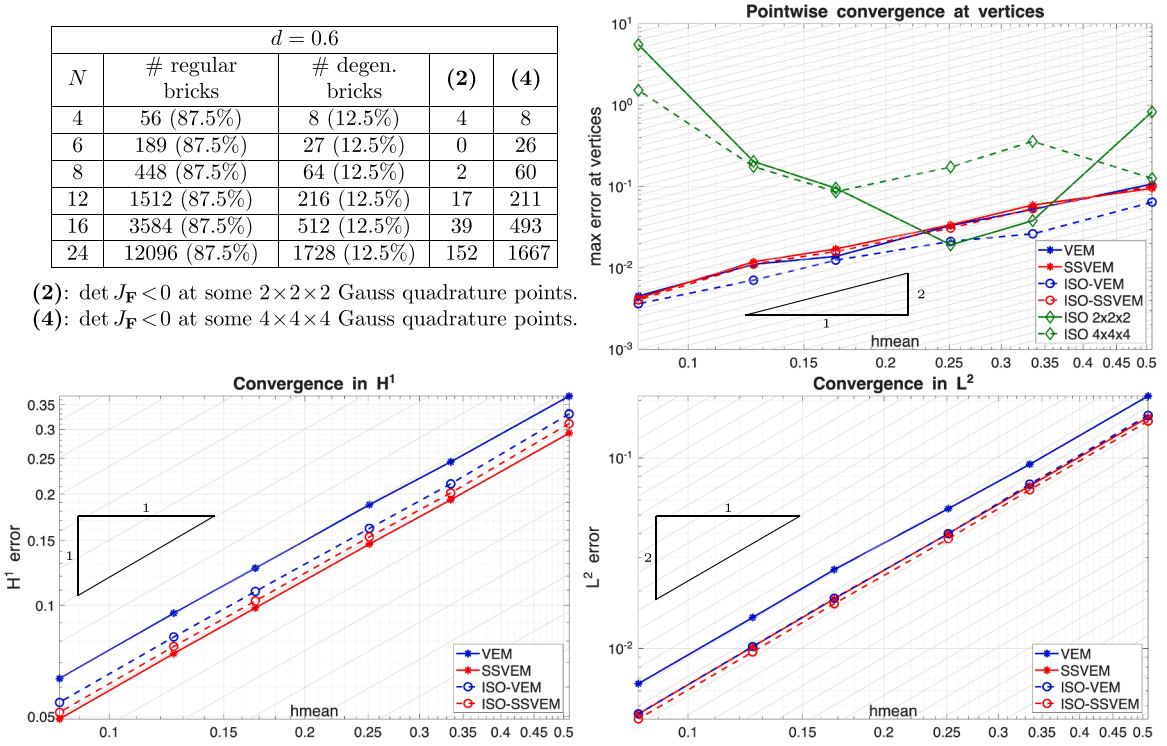

Fig. 12. Distortion $d = 0.6$.

$d = 0.8$				
N	# regular bricks	# degen. bricks	**(2)**	**(4)**
4	55 (85.9%)	9 (14.1%)	8	8
6	177 (81.9%)	39 (18.1%)	25	30
8	423 (82.6%)	89 (17.4%)	57	71
12	1431 (82.8%)	297 (17.2%)	204	236
16	3411 (83.3%)	685 (16.7%)	454	550
24	11494 (83.1%)	2330 (16.9%)	1560	1844

(2): $\det J_{\mathbf{F}} < 0$ at some $2\times2\times2$ Gauss quadrature points.
(4): $\det J_{\mathbf{F}} < 0$ at some $4\times4\times4$ Gauss quadrature points.

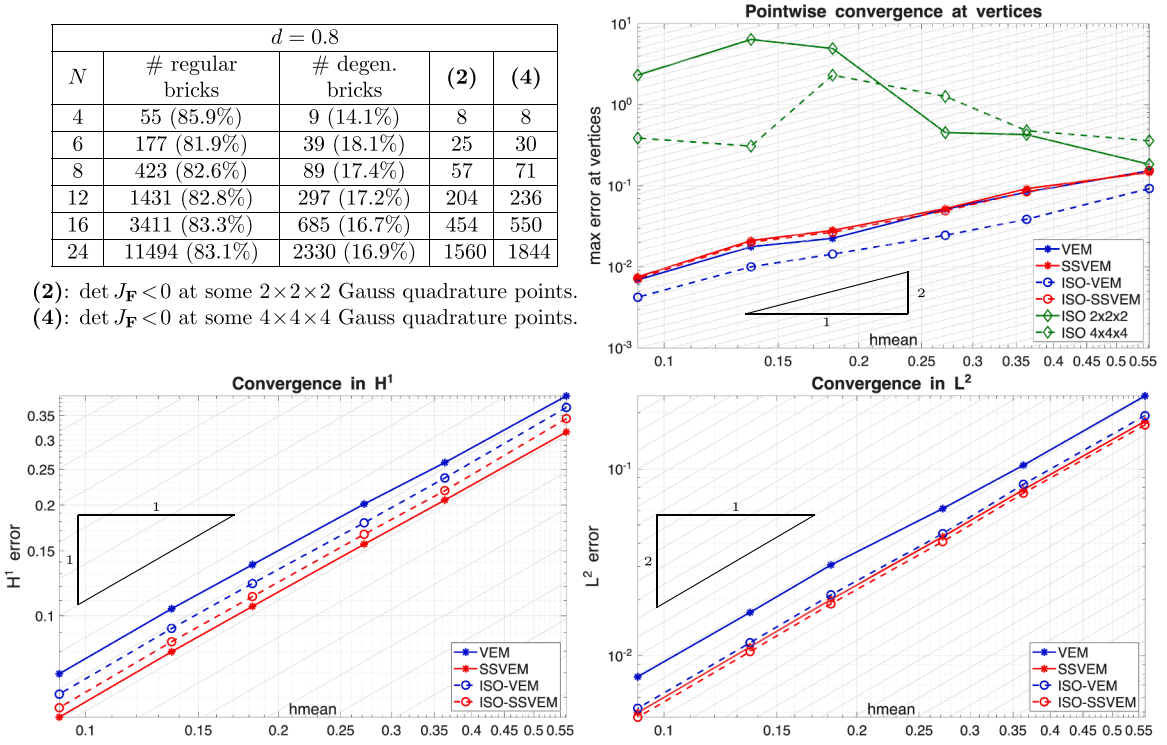

Fig. 13. Distortion $d = 0.8$.

$d = 0.9$				
N	# regular bricks	# degen. bricks	**(2)**	**(4)**
4	51 (79.7%)	13 (20.3%)	8	9
6	172 (79.6%)	44 (20.4%)	27	37
8	404 (78.9%)	108 (21.1%)	64	82
12	1368 (79.2%)	360 (20.8%)	216	286
16	3246 (79.2%)	850 (20.8%)	512	660
24	10958 (79.3%)	2866 (20.7%)	1728	2225

(2): $\det J_{\mathbf{F}} < 0$ at some $2\times2\times2$ Gauss quadrature points.
(4): $\det J_{\mathbf{F}} < 0$ at some $4\times4\times4$ Gauss quadrature points.

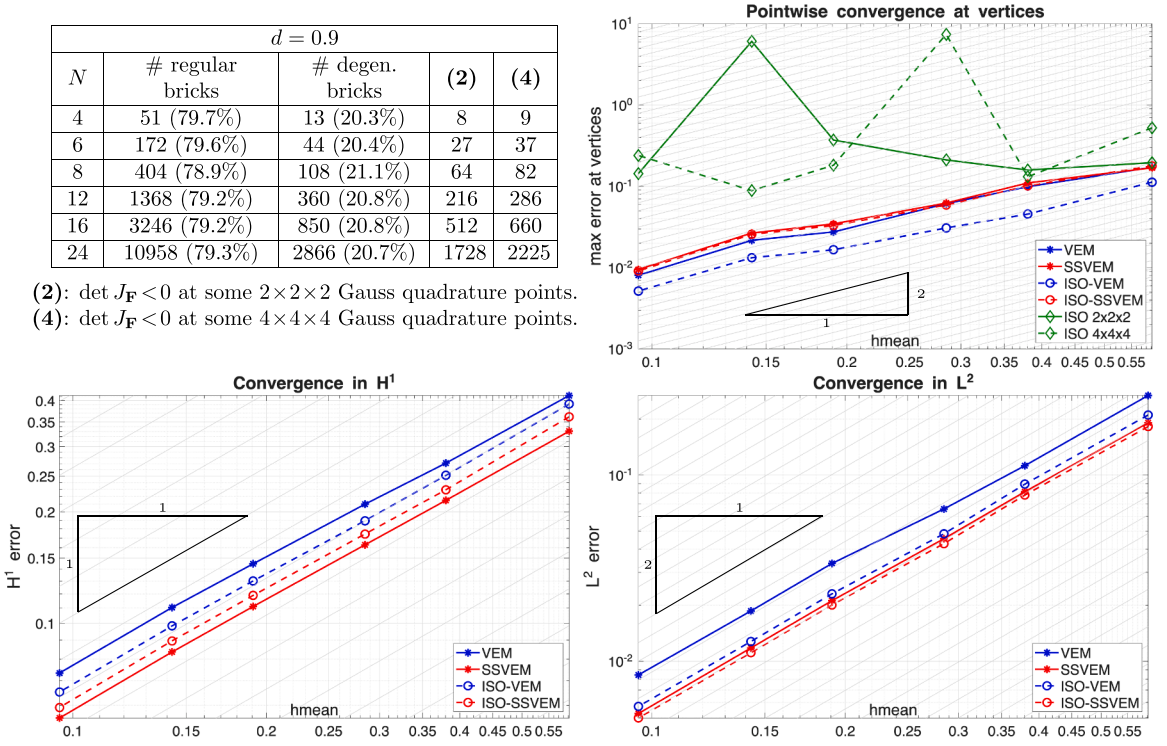

Fig. 14. Distortion $d = 0.9$.

8. Numerical experiments

For the numerical experiments we consider problem (39) with the following coefficients:

$$\mathsf{D} = \begin{bmatrix} x^2+1 & xy & xz \\ xy & y^2+1 & yz \\ xz & yz & z^2+1 \end{bmatrix}, \quad c = x^2 + y + \log(2+z)$$

and known solution

$$u_{\text{ex}} = y\sin(3xz) - \log(2 + x^2 + y^4 + z^2) + [\cos(x + \exp(y) + z)]^2.$$

The data f and g are chosen so that u_{ex} is the exact solution of (39).

The objective of the numerical experiments is to show that when a brick element becomes too distorted for reliable isoparametric finite element treatment, it can be seamlessly replaced by a virtual element, without compromising compatibility with the standard isoparametric formulation.

To control the distortion of the virtual bricks and prevent the creation of self-intersecting elements, the meshes are generated as follows.

We consider sequences of meshes with decreasing mesh size, each parameterized by a distortion factor d between 0 and 1, which governs the magnitude of the applied distortion. Starting from a uniform partition of the computational domain $\Omega = [0,1]^3$ into $N \times N \times N$ cubes (with N even), we group each block of $2 \times 2 \times 2$ cubes and perturb its central vertex according to d. More precisely, we define a concentric cube centered in the block at a (normalized) distance d from its center, and select a point on its surface as the new position of the central vertex. The point is chosen randomly, with a bias toward locations near the vertices of the concentric cube, in order to increase the geometric distortion.

When $d = 0$, blocks are not distorted and the mesh is just a uniform cube mesh composed of elements with side length $1/N$. When d increases, the elements become more and more distorted.

In Fig. 7 the procedure is shown in the two-dimensional case. The concentric cube at distance d from the center is drawn in red and the region where the new vertex is chosen randomly is thickened. A resulting $2 \times 2 \times 2$ block of bricks in three dimensions is shown in Fig. 8.

In Figs. 9– 14, we report the numerical experiments obtained for increasing values of the distortion parameter d, comparing the six methods shown in Table 1.

For each value of d, in the first panel we present a table summarizing key features of the corresponding mesh sequence. The second and third columns report the numbers of regular and degenerate bricks, respectively; the degeneracy test is implemented according to the algorithm described in [36]. The fourth and fifth columns list the numbers of bricks for which the Jacobian determinant becomes negative at one or more Gauss quadrature points, for the $2 \times 2 \times 2$ and $4 \times 4 \times 4$ integration schemes, respectively.

In the second panel, the maximum error at the vertices is plotted for all methods. It is observed that, whenever the Jacobian determinant becomes negative at some Gauss quadrature points, the isoparametric scheme fails. Therefore, as it is well known, the isoparametric formulation proves unreliable for degenerate brick elements.

In the third and fourth panel, we plot the L^2 and H^1 errors for the pure VEM and the mixed isoparametric–VEM schemes (each with the two possible VEM stabilization strategies). The results demonstrate remarkable robustness, even for highly distorted elements.

The L^2 and H^1 errors for the isoparametric formulation are meaningless for degenerate bricks and are therefore omitted from the third and fourth panels.

For $d = 0$ and $d = 0.2$, no degenerate bricks are present; consequently, the ISO–VEM and ISO–SSVEM schemes yield identical solutions, which coincide with the pure isoparametric results.

The numerical experiments presented here provide clear evidence that the Virtual Element Method is able to handle highly degenerate brick elements with curved faces in a stable and accurate manner. Moreover, they confirm that the method can be employed in combination with the standard Isoparametric Finite Element Method without any loss of consistency or compatibility, thereby ensuring a seamless integration of the two approaches within the same computational framework.

9. Conclusions

We have presented a new 8-node, order 1, hexahedral VE with curved faces, named "virtual brick". The element is intended to replace the standard 8-node, trilinear isoparametric FE bricks in a FE mesh, whenever a suitable indicator suggests that the brick distortion exceeds a "safety limit". In such cases, the element would be either degenerate, thus leading the simulation to fail, or excessively distorted, thus resulting in an unacceptable loss of accuracy.

The proposed method is developed with reference to a simple thermal problem with a reaction term. The main features of the proposed virtual brick are as follows.

- The virtual brick is defined as a solid with six quadrilateral faces that are each a bilinear transformation of the reference square, without making use of the trilinear mapping of the element interior.
- The virtual brick is based on the same degrees of freedom of the standard 8-node isoparametric $\mathbb{Q}_1$ FE brick. Furthermore, the functional space on the faces is also the same, allowing for a seamless incorporation in a FE mesh, replacing excessively distorted FEs, while maintaining the FE bricks elsewhere.

- Volume and surface integrals on the virtual brick can be computed using the standard quadrature rules based on Gauss points, commonly used in the FEM, even in the degenerate case. This is of utmost importance in the case of nonlinear problems, where the material behavior is enforced at these points, and also greatly simplifies the incorporation of the virtual bricks in the element library of existing commercial FE codes. However, while preliminary numerical experiments are encouraging, it should be emphasized that a rigorous assessment of the accuracy of standard quadrature rules in the degenerate case is still missing.
- The virtual brick enjoys the typical robustness with respect to mesh distortion exhibited by the other types of VEs existing in the literature.

The following properties characterize the virtual brick.

- The faces of a virtual brick can be arbitrarily distorted as long as their mapped geometries do not intersect with each other. The functional space inside the element volume is "virtual", i.e., not explicitly defined.
- A self-stabilized version, i.e., without requiring an explicit stabilization term, is presented. The self-stabilization is achieved by projecting the gradient of the virtual functions onto the gradient of cubic harmonic polynomials.
- In the special case that the self-stabilized virtual brick is a rectangular parallepiped, its stiffness matrix exactly coincides with that of the standard $\mathbb{Q}_1$ isoparametric FE cube.
- For the integration of virtual functions, a least-squares quadrature formula with nodes at the vertices has been provided, which is exact for polynomials of degree 1.
- First order convergence of the method in the H^1 norm has been shown to hold for different types of numerical integration of the loading term.

Numerical tests with different distortion levels have confirmed that the virtual brick provides the same results as the standard isoparametric $\mathbb{Q}_1$ FE in the case of regular brick elements, while excellent performances have been obtained also in the case of severe distortions, even beyond the degeneration limit, where the standard isoparametric $\mathbb{Q}_1$ FE fails. In addition, full compatibility of the virtual brick with isoparametric $\mathbb{Q}_1$ FE has been assessed in the case of meshes containing regular FE bricks and highly distorted virtual bricks.

The formulation of a virtual brick for solid mechanics nonlinear problems is in progress and will be presented in a forthcoming paper.

CRediT authorship contribution statement

M. Cremonesi: Writing - original draft; **F. Dassi:** Writing - original draft; **C. Lovadina:** Writing - original draft; **U. Perego:** Writing - original draft; **A. Russo:** Writing - original draft.

Data availability

Data will be made available on request.

Declaration of competing interest

The authors declare that they have no known competing financial interests or personal relationships that could have appeared to influence the work reported in this paper.

Acknowledgments

M.C., U.P. and A.R. have been partially supported by the Italian Ministry of University and Research through the project PRIN2022 PNRR “Polyhedral Galerkin methods for engineering applications to improve disaster risk forecast and management: stabilization-free operator preserving methods and optimal stabilization methods” (PRIN2022 PNRR - P2022BH5CB, CUP D53D23018840001: UE funding – NextGenerationEU – mission 4, component 2, investment 1.1). C.L., F.D. and A.R. are members of the INdAM Research Group GNCS and acknowledge partial support from INdAM-GNCS.

References

[1] J.F. Shepherd, C.R. Johnson, Hexahedral mesh generation constraints, Eng. Comput. 24 (2008) 195–213. https://doi.org/10.1007/s00366-008-0091-4
[2] N. Pietroni, M. Campen, A. Sheffer, G. Cherchi, D. Bommes, X. Gao, R. Scateni, F. Ledoux, J.F. Remacle, M. Livesu, Hex-Mesh generation and processing: a survey, ACM Trans. Graph. 42 (2022). https://doi.org/10.1145/3554920
[3] T. Blacker, Automated conformal hexahedral meshing constraints, challenges and opportunities, Eng. Comput. 17 (2001) 201–210. https://doi.org/10.1007/PL00013384
[4] N.S. Lee, K.J. Bathe, Effects of element distortions on the performance of isoparametric elements, Int. J. Numer. Methods Eng. 36 (1993) 3553–3576. https://doi.org/10.1002/nme.1620362009
[5] G. Castellazzi, On the performances of parametric finite elements when geometry distortions occur, Finite Elem. Anal. Des. 47 (2011) 1306–1314. https://doi.org/10.1016/j.finel.2011.07.004
[6] J.R. Shewchuk, What is a good linear element? interpolation, conditioning, and quality measures, in: 11Th International Meshing Roundtable. Sandia National Laboratories, 2002, pp. 115–126.
[7] P.M. Knupp, Algebraic mesh quality metrics, SIAM J. Sci. Comput. 23 (2001) 193–218. https://doi.org/10.1137/S1064827500371499

[8] M. Livesu, A. Sheffer, N. Vining, M. Tarini, Practical hex-Mesh optimization via edge-cone rectification, ACM Trans. Graph. 34 (2015). https://doi.org/10.1145/2766905

[9] P. Wriggers, J. Korelc, On enhanced strain methods for small and finite deformations of solids, Comput. Mech. 18 (1996) 413–428. https://doi.org/10.1007/BF00350250

[10] P. Lei Zhou, S. Cen, J.B. Huang, C.F. Li, Q. Zhang, An unsymmetric 8-node hexahedral element with high distortion tolerance, Int. J. Numer. Methods Eng. 109 (2017) 1130–1158. https://doi.org/10.1002/nme.5318

[11] B. Prabhune, K. Suresh, A computationally efficient isoparametric tangled finite element method for handling inverted quadrilateral and hexahedral elements, Comput. Methods Appl. Mech. Eng. 405 (2023) 115897. https://doi.org/10.1016/j.cma.2023.115897

[12] L. Beirão da Veiga, F. Brezzi, A. Cangiani, G. Manzini, L.D. Marini, A. Russo, Basic principles of virtual element methods, Math. Models Methods Appl. Sci. 23 (1) (2013) 199–214. https://doi.org/10.1142/S0218202512500492

[13] L. Beirão da Veiga, F. Brezzi, L.D. Marini, A. Russo, The virtual element method, Acta Numerica 32 (2023) 123–202. https://doi.org/10.1017/S0962492922000095

[14] L. Beirão da Veiga, F. Dassi, A. Russo, High-order virtual element method on polyhedral meshes, Comput. Math. Appl. 74 (5) (2017) 1110–1122. https://doi.org/10.1016/j.camwa.2017.03.021

[15] D. Prada, F. Brezzi, L.D. Marini, A Virtual Element Method on polyhedra with curved faces, (2025). arXiv:2509.23005

[16] L. Beirão da Veiga, Y. Liu, L. Mascotto, A. Russo, The nonconforming virtual element method with curved edges, J. Sci. Comput. 99 (1) (2024) 35.

[17] R.L. Taylor, E. Artioli, VEM For inelastic solids, Comput. Method. Appl. Sci. 46 (2018) 381–394. https://doi.org/10.1007/978-3-319-60885-3_18

[18] F. Aldakheel, B. Hudobivnik, E. Artioli, L.B.d. Veiga, P. Wriggers, Curvilinear virtual elements for contact mechanics, Comput. Methods Appl. Mech. Eng. 372 (2020) 113394. https://doi.org/10.1016/J.CMA.2020.113394

[19] E. Artioli, L.B.d. Veiga, M. Verani, An adaptive curved virtual element method for the statistical homogenization of random fibre-reinforced composites, 2020. https://doi.org/10.1016/j.finel.2020.103418

[20] D. Sun, E. Pescialli, Q. Li, M. Cremonesi, C. Lovadina, U. Perego, A. Russo, Deltahedral self-stabilized virtual elements for 3d linear elastostatics problems, Comput. Mech. 76 (2025) 727–743. https://doi.org/10.1007/s00466-025-02622-4

[21] A.L. Gain, C. Talischi, G.H. Paulino, On the virtual element method for three-dimensional linear elasticity problems on arbitrary polyhedral meshes, Comput. Methods Appl. Mech. Eng. 282 (2014) 132–160. https://doi.org/10.1016/J.CMA.2014.05.005

[22] K. Park, H. Chi, G.H. Paulino, On nonconvex meshes for elastodynamics using virtual element methods with explicit time integration, Comput. Methods Appl. Mech. Eng. 356 (2019) 669–684. https://doi.org/10.1016/J.CMA.2019.06.031

[23] H. Chi, L.B.d. Veiga, G.H. Paulino, Some basic formulations of the virtual element method (VEM) for finite deformations, Comput. Methods Appl. Mech. Eng. 318 (2017) 148–192. https://doi.org/10.1016/J.CMA.2016.12.020

[24] B.B. Xu, W.L. Fan, P. Wriggers, High-order 3d virtual element method for linear and nonlinear elasticity, Comput. Methods Appl. Mech. Eng. 431 (2024) 117258. https://doi.org/10.1016/J.CMA.2024.117258

[25] B.B. Xu, L.B.d. Veiga, Y.J. Zhang, P. Wriggers, Second order three-dimensional serendipity virtual elements for hyperelasticity: static and dynamic analysis, Comput. Methods Appl. Mech. Eng. 448 (2026) 118432. https://doi.org/10.1016/j.cma.2025.118432

[26] F. Aldakheel, B. Hudobivnik, P. Wriggers, Virtual elements for finite thermo-plasticity problems, Comput. Mech. 64 (2019) 1347–1360. https://doi.org/10.1007/s00466-019-01714-2

[27] B. Hudobivnik, F. Aldakheel, P. Wriggers, A low order 3d virtual element formulation for finite elasto–plastic deformations, Comput. Mech. 63 (2019) 253–269. https://doi.org/10.1007/S00466-018-1593-6/FIGURES/20

[28] C. Mertcan, B. Hudobivnik, F. Aldakheel, P. Wriggers, 3D mixed virtual element formulation for dynamic elasto-plastic analysis, Comput. Mech. 68 (2021) 1–18. https://doi.org/10.1007/s00466-021-02010-8

[29] D. van Huyssteen, B.D. Reddy, The incorporation of mesh quality in the stabilization of virtual element methods for nonlinear elasticity, Comput. Methods Appl. Mech. Eng. 392 (2022) 114720. https://doi.org/10.1016/J.CMA.2022.114720

[30] A.M. D'Altri, S. de Miranda, L. Patruno, E. Sacco, An enhanced VEM formulation for plane elasticity, Comput. Methods Appl. Mech. Eng. 376 (2021) 113663. https://doi.org/10.1016/j.cma.2020.113663

[31] A. Lamperti, M. Cremonesi, U. Perego, A. Russo, C. Lovadina, A hu–washizu variational approach to self-stabilized virtual elements: 2d linear elastostatics, Comput. Mech. 71 (2023) 935–955. https://doi.org/10.1007/s00466-023-02282-2

[32] S. Berrone, A. Borio, D. Fassino, F. Marcon, Stabilization-free virtual element method for 2d second order elliptic equations, Comput. Methods Appl. Mech. Eng. 438 (2025) 117839. https://doi.org/10.1016/j.cma.2025.117839

[33] B.B. Xu, P. Wriggers, 3D stabilization-free virtual element method for linear elastic analysis, Comput. Methods Appl. Mech. Eng. 421 (2024) 116826. https://doi.org/10.1016/J.CMA.2024.116826

[34] T. Bouchez, A. Gravouil, N. Blal, A. Giacoma, E. Delor, J.D. Beley, A hu–washizu stabilization-free virtual element method for 3d linear elasticity with star-convex polyhedrons, Comput. Methods Appl. Mech. Eng. 432 (2024) 117420. https://doi.org/10.1016/j.cma.2024.117420

[35] G. Leoni, A First Course in Sobolev Spaces, Graduate studies in mathematics, American Mathematical Society, 2009. https://books.google.it/books?id=eE2ZAwAAQBAJ.

[36] A. Johnen, J.C. Weill, J.F. Remacle, Robust and efficient validation of the linear hexahedral element, Procedia Eng. 203 (2017) 271–283. Proceedings of the 26th International Meshing Roundtable (IMR26), 18–21 September 2017, Barcelona, Spain. https://doi.org/10.1016/j.proeng.2017.09.809

[37] P.M. Knupp, On the invertibility of the isoparametric map, Comput. Methods Appl. Mech. Eng. 78 (3) (1990) 313–329. https://doi.org/10.1016/0045-7825(90)90004-6

[38] L. Beirão da Veiga, F. Brezzi, L.D. Marini, A. Russo, The hitchhiker's guide to the virtual element method, Math. Models Methods Appl. Sci. 24 (8) (2014) 1541–1573. https://doi.org/10.1142/S021820251440003X

[39] B. Ahmad, A. Alsaedi, F. Brezzi, L.D. Marini, A. Russo, Equivalent projectors for virtual element methods, Comput. Math. Appl. 66 (3) (2013) 376–391. https://doi.org/10.1016/j.camwa.2013.05.015

[40] M. Giaquinta, G. Modica, J. Soucek, Cartesian Currents in the Calculus of Variations I: Cartesian Currents, 37 of *Ergebnisse der Mathematik und ihrer Grenzgebiete. 3. Folge / A Series of Modern Surveys in Mathematics*, Springer Berlin Heidelberg, Berlin, Heidelberg, Berlin, Heidelberg, 1998.

[41] P.D. Lax, Change of variables in multiple integrals, Am. Math. Month. 106 (6) (1999) 497–501. https://doi.org/10.1080/00029890.1999.12005078

[42] S. Berrone, A. Borio, F. Marcon, A stabilization-free virtual element method based on divergence-free projections, Comput. Methods Appl. Mech. Eng. 424 (2024) 116885. https://doi.org/10.1016/j.cma.2024.116885

[43] S. Axler, P. Bourdon, W. Ramey, Harmonic Function Theory, Springer, New York, 2nd edition, New York, 2001.